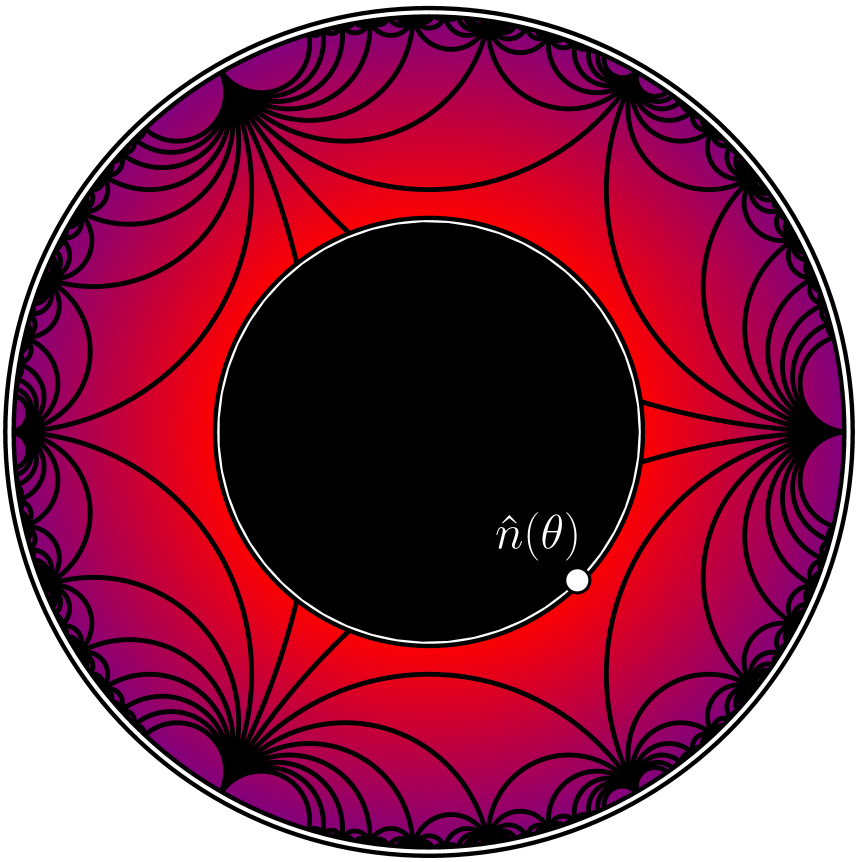

Fermi Surfaces of Holographic Metals

Holographic Effective Field Theory of non-Fermi Liquids at Finite Temperature

Master's thesis in Physics

ELI ISMAILOV

DEPARTMENT OF PHYSICS
CHALMERS UNIVERSITY OF TECHNOLOGY
Gothenburg, Sweden 2024
www.chalmers.se

Master's thesis 2024

Fermi Surfaces of Holographic Metals

Holographic Effective Field Theory of non-Fermi Liquids at Finite Temperature

Eli Ismailov

CHALMERS
UNIVERSITY OF TECHNOLOGY

Department of Physics
Division of Subatomic, High Energy- and Plasma Physics
Chalmers University of Technology
Gothenburg, Sweden 2024

Fermi Surfaces of Holographic Metals:
Holographic Effective Field Theory of non-Fermi Liquids at Finite Temperature.

Eli Ismailov

Supervisor: Eric Nilsson, Department of Physics
Examiner: Ulf Gran, Department of Physics

Master's Thesis 2024
Department of Physics
Division of Subatomic, High Energy- and Plasma Physics

Chalmers University of Technology
SE-412 96 Gothenburg
Telephone: +46 31 772 1000

Cover: Illustration of the AdS/CFT correspondence of a non-Fermi liquid. The figure is made in Mathematica using code based on Ref. [1].

Typeset in LaTeX
Printed by Chalmers Digital Printing
Gothenburg, Sweden 2024

Fermi Surfaces of Holographic Metals:
Holographic Effective Field Theory of non-Fermi Liquids at Finite Temperature.

Eli Ismailov
Department of Physics
Chalmers University of Technology

Abstract

One of the most challenging endeavours in theoretical condensed matter physics is solving models of strongly correlated metals. In these systems, the standard techniques from Fermi liquid theory have limited applicability, necessitating new descriptions. One particularly promising approach is known as holographic duality, which conjectures a relation between the seemingly unapproachable physics of strongly coupled quantum field theories and classical gravitational theories in one higher dimension. While successful in many regards, the usual holographic approach for metals fails to incorporate a satisfactory description of a Fermi surface, an indisputably important ingredient for any theory describing a metal. Specifically, any theory of a metal ought to have a Fermi surface that satisfies Luttinger's theorem. In this thesis, we introduce a holographic model that exhibits the necessary behaviour of metal. Diverging from the typical holographic treatment where all scales are described, we instead assume the dual theory to be an infrared effective field theory. We explore the behaviour of the theory across various temperatures by numerically solving the differential equations of motion for the gravity theory. Motivated by the numerical predictions, we suggest a UV cutoff scale for the theory. We discuss some potential limitations and plausible modifications of the model.

Keywords: Holographic EFT, AdS/CFT correspondence, Fermi surface, ersatz Fermi liquid.

Acknowledgements

I want to extend my heartfelt thanks to my supervisor, Eric Nilsson, for guiding me throughout these six months. You have been incredibly generous with your time and effort, and your enthusiasm for the subject has continuously inspired and motivated me.

Furthermore, I would like to thank Ulf Gran for providing me with the opportunity to undertake this project and for facilitating what has become my most enjoyable experience in physics.

I am also thankful to the dark matter crowd—Andreas Lund, Gustav Strandlycke, and Thomas Jerkvall-for the great company and for enduring my ramblings.

Finally, I would like to express my deepest gratitude to my family for your support. What is noumenal cannot be captured in words, but I hope you can sense my appreciation.

Eli Ismailov, Gothenburg, June 2024

Table of contents

List of figures

1. Introduction

In the age-old quest to understand the phenomenological world's behaviour, no framework has been as successful as quantum field theory (QFT). Since its inception in the early 20th century, it has had a remarkable ability to predict the behaviour of various phenomena using the language of fields. At the core of quantum field theory lies the interactions of fields among themselves and with other fields [2]. The interactions are quantified by a parameter known as the coupling constant, the magnitude of which essentially determines the strength of various interactions.

While the foundational idea behind the interactions in quantum field theories given by this naive description might seem straightforward, the calculations themselves are usually impossibly complex. To deal with these complexities, physicists often turn to perturbation theory, which tackles the problem by expressing interactions as a series of expansions in the coupling constant [3]. For weakly interacting theories, the small coupling constant ensures that the series expansion of the interaction converges quickly. Thus, perturbation theory has proven to be highly successful in weakly coupling theories [4].

The perturbative venture becomes increasingly untenable as we turn up the coupling constant dial. The higher-order terms in the expansion can become as impactful, if not more, than those at lower order. Perturbation theory thus loses its efficacy when applied to strongly interacting theories [5]. As nature has it, some systems seem to be strongly coupled, falling outside of the capacities of perturbation theory and requiring new tools. The prime example of strong coupling physics where perturbation theory is limited in scope is quantum chromodynamics (QCD), which deals with quarks and gluons. Another set of systems, which are the main focus of this thesis, are strongly correlated metals. Strong electron correlations disrupt the typical approach of Fermi liquid theory [6] used for conventional metals where correlation is weak. These systems are collectively referred to as non-Fermi liquids [7]. Experimental observations have confirmed non-Fermi liquid behaviour in several materials [8–10]. A category within non-Fermi liquids is that of "*strange metals*", which are especially notable for their linear-in-temperature resistivity in contrast to the T^2 dependence observed in conventional metals described by Fermi liquid theory [11]. The strange metal phase is prominently featured in the temperature-doping phase diagram of high-temperature cuprates [12]. In total, significant interest has spurred for the development of a coherent theory that can unveil the underlying physics of these materials.

The following question arises: how do we accurately describe the physics in strongly correlated systems where the conventional approaches no longer hold? A strong

contender emerged at the turn of the century, now known as "*holographic duality*". Originating from string theory, holographic duality, specifically in the form of the AdS/CFT correspondence, bridges the complex quantum realm with the more tractable theories of classical gravity. It suggests that the physics of certain strongly coupled quantum systems are dual to a higher-dimensional weakly coupled gravitational theory. Using a dictionary to translate between the two theories, one finds that the impenetrable problems in quantum field theories can be translated into the solvable framework of classical gravity.

1.1 The AdS/CFT correspondence

In 1997, Juan Maldacena published a paper where he presented a revolutionary duality [13]. He showed how type IIB string theory on $AdS_5 \times S^5$ is dual to a strong coupling 3+1 $\mathcal{N} = 4$ super-Yang-Mills theory with a large U(N) gauge group. He further conjectured that various compactifications of M/string theory on Anti-de Sitter (AdS) spacetimes are dual to various conformal field theories (CFTs).

This idea was formalised by Gubser, Klebanov and Polyakov [14], and independently by Witten [15], who provided a more general mathematical foundation for this duality. They gave an equality between the partition functions at certain limits, enabling the translation of results from one theory to the other, essentially allowing for a dictionary to navigate between the two landscapes of super-gravity and CFTs in lower dimensions. The phrase holographic duality naturally fits this procedure of going down in dimensions. The analogy comes from holography in optics, where a three-dimensional object is encoded on a two-dimensional surface. Similarly, the AdS/CFT correspondence suggests that a $D + 1$ dimensional gravitational theory (the bulk theory) can be fully described by a D dimensional conformal field theory living on its boundary [16].

A question then arises as to what the extra radial dimension in the gravity theory corresponds to in the CFT living in one dimension less. It turns out to correspond to the renormalisation group (RG). This analogy suggests that variations in the energy scale of the CFT are mirrored by movements along the radial dimension in the bulk. Thus, delving into the radial dimension of the bulk allows one to trace the RG flow [17].

For the AdS/CFT correspondence, there are two approaches to constructing holographic dualities. These are referred to in the literature as "top-down" and "bottom-up" methodologies [17]. The top-down method approaches the theory at a foundational level, starting with a string theory, compactifying on some manifold, and arriving at a bulk action that is dual to some QFT. Thus, the QFT is arrived at by constraining a more general overarching theory of gravity; this was the approach originally used in Refs. [13–15]. Conversely, the bottom-up approach, which is generally the approach used when modelling condensed matter systems [18], begins at the other end. The bulk action is postulated based on the qualities wished for in the dual QFT.

The meaning of *conformal* in conformal field theory signifies the additional symmetry of invariance under all mappings that locally preserves angles but not necessarily distances. In the bottom-up approach, it is convenient for the CFT to be in the large N limit, where N refers to the rank of matrix-valued fields within the CFT. In this limit, the stringy aspects of quantum gravity in AdS space simplify to classical general relativity, giving a tangible bridge between strongly coupled quantum fields and spacetime geometry [17, 18]. This thesis will use the bottom-up approach to construct a gravity theory dual to a QFT in the large N limit, which describes metals. By construction, this approach allows us to stay within the realm of classical physics.

1.2 Fermi surfaces in holography

The hope is that the AdS/CFT correspondence offers a novel perspective on examining strongly correlated fermionic materials, classified as non-Fermi liquids, that are inaccessible to traditional methods. Using the bottom-up approach requires precision to ensure that the correct physics is encoded in the dual theory. To get an idea of what constituents are necessary, we can start with the simplest metal possible, the Fermi gas. A Fermi gas is a system of non-interacting fermions. We find the ground state of this system by filling up all the lowest energy states until we have accounted for all fermions while adhering to the Pauli exclusion principle. This gives an enclosed volume in momentum space, which is referred to as the Fermi sea. Using a sea as an analogy, the states can be thought of as the water in the sea filling up the ocean floor. The Fermi surface is the boundary in momentum space that separates these occupied states from the unoccupied ones. All low-energy excitations are fermions that leave the sea or create holes within it. Building on our analogy with water, these can be thought of as the ripples on the surface or bubbles underneath.

By adding an interacting term in the Hamiltonian with a small coupling constant, weak interactions can be turned on; we enter the territory of Fermi liquids. The simple picture for the Fermi surface of the non-interacting case no longer holds as the eigenstates of the Hamiltonian are altered by the interactions [19]. One can still construct a ground state regardless, albeit one that differs from the previous one. The excitations from this interacting ground state consist of the particle excitations and the interactions they drag along. When these excitations are long-lived, they are called *quasiparticles*. The Fermi surface in Fermi liquid theory is the surface in momentum space around which the quasiparticles have a long lifetime. When the interaction strength is increased, the quasiparticles thermalise much quicker, meaning that the lifetime of the quasiparticles is reduced. Therefore, in strongly interacting theories, quasiparticles can no longer be said to exist, which is precisely the case for non-Fermi liquid theory [20]. Since Fermi liquid theory depends on quasiparticles, non-Fermi liquids require a different description. While quasiparticles are missing, the Fermi surface remains and is thus a necessary component to the physics of non-Fermi liquids [21].

When using the AdS/CFT correspondence to model non-Fermi liquids, the usual procedure involves using a classical Reissner–Nordström bulk as the dual of a certain

QFT. The QFT is perturbed by a chemical potential, giving a non-zero charge density. In the bulk, this is captured by the time component of the gauge field. In such a way, non-trivial quantities of strongly correlated condensed matter systems can be obtained, attesting to the abilities of the methodology [17]. However, it also has shortcomings; a serious issue is the lack of a valid Fermi surface [21], something that is pivotal to understanding the physics of metals. The meaning of "valid" in this context is understood through Luttinger's theorem [22], which gives a proportional relation between the area of the Fermi sea and the charge density of the system. While Luttinger's theorem originates from the weakly correlated Fermi liquid theory, it ought to hold for non-Fermi liquids as well [23]. For the Reissner–Nordström model, the charge in the bulk disappears behind the horizon [24], thereby violating Luttinger's theorem due to the unaccounted charge. The emergence of a Fermi surface compliant with Luttinger's theorem is possible upon incorporating quantum gravity corrections into the gravitational theory [25, 26]. This consideration somewhat detracts from the holographic approach's initial allure, whereby solving simpler classical physics achieves an understanding of strongly coupled systems.

1.3 Outline

All the work done in this thesis is based on Ref. [21] where a holographic model for a non-Fermi liquid is constructed using the framework presented in Ref. [23]. This thesis aims to extend this prior work numerically to see how the behaviour changes at finite temperatures. This will be done after introducing the necessary prerequisites for the model.

Chapter 2, introduces the holographic duality. It begins with a short review of the necessary holographic concepts needed for this thesis. First, we explain Anti-de Sitter space, which forms the backdrop for the holographic models. We then discuss correlation functions and their computation within this framework. Subsequently, the holographic dictionary is introduced, enabling the translation between the bulk gravitational theory and a boundary quantum field theory. Specific topics covered include Anti-de Sitter space, correlation functions, the holographic dictionary, bulk fields and sources, the radial dimension, incorporating temperature, and a basic example of a massive scalar field as a reference for the holographic calculations to come in chapter 3.

Chapter 3 focuses on the theoretical underpinnings of classifying metals and their specific characteristics, leading to the introduction of ersatz Fermi liquids. We introduce Luttinger's theorem, which provides a fundamental relation between the Fermi surface and the charge density. Next, we describe how to incorporate a metal's essential properties into a holographic model using the insights from Chapter 2. The chapter concludes by explicitly solving the holographic model for a non-Fermi liquid at zero temperature.

Chapter 4 transitions from the analytical evaluations of prior work to instead evaluating the same metallic model which concluded chapter 3 at finite temperature

using a numerical method called the pseudospectral algorithm. Upon obtaining a solution, we examine the differences between the behaviours at zero and finite temperatures.

Chapter 5 concludes the thesis with a discussion regarding topics for future research. Specifically, we discuss how to address the emergence of infinite DC conductivity and how to incorporate metric-gauge field couplings.

Conventions and notations

This thesis uses the mostly plus convention for the metric $(-,+,+,+)$, as is common in holography. To make calculations as concise as possible, we work in natural units where $c = \hbar = k_{\mathrm{B}} = 1$. It is necessary to distinguish between bulk and boundary expressions, a distinction which is particularly important for the gauge fields A_μ and actions S. Therefore, in the bulk theory, upright A_μ is used for the gauge fields and S for the actions. For the boundary theory, I is used for the actions and a calligraphic $\mathcal{A}_\mu$ for the gauge fields. This distinction is maintained in chapters discussing holography. In chapter 3 up until section 3.2, this distinction is not made, as the topic of discussion will be general field theory. Lastly, let us comment on how indices are used. The manifold considered varies from section to section, and the dimension over which the indices range should be clear from the context. Generally, upright Latin letters $A, B, C, \ldots$ are used when θ is included. Greek letters $\mu, \nu, \rho, \ldots$ are used instead when θ is excluded. Lowercase Latin letters i, j are used when the spatial dimensions x and y are considered.

2. Holographic duality

In this chapter, we introduce the necessary machinery to describe aspects of QFTs using classical gravity. We begin by introducing the prerequisites, which are the geometry of the correspondence and how to make field theory calculations. The concept of the holographic dictionary is introduced, allowing us to interpret boundary phenomena in terms of bulk dynamics. Specifically, this is done using a relation known as the GKPW rule, which allows for correlation functions in the QFT to be computed using the bulk theory.

Having established the connection between the boundary and the bulk, we show specific correspondences between the bulk fields and sources in the boundary theory. Thereafter, we underline the significance of the radial dimension in the bulk as it corresponds to the renormalisation group in the boundary theory. Finally, we show how thermodynamics can be manifest despite the boundary theory being a CFT. Having established the rules, we give a simple example known as the canonical example. This should clarify the standard procedure when making holographic calculations, as the same approach will be used in the next chapter, where we will apply the same line of thinking to theories of metals.

This chapter is far from a complete description of the holographic bottom-up approach. It will merely establish the necessary holographic prerequisites for this thesis's aim. For a more comprehensive understanding of the bottom-up approach in condensed matter physics through the lens of holography, readers should refer to the literature cited throughout this chapter, specifically Refs. [17, 18].

2.1 Anti-de Sitter space

Before doing anything, we need to set the stage for where the physics lives. Abbreviated as AdS in the name of the correspondence, the gravity theory takes place in so-called Anti-de Sitter space. Anti-de Sitter space is a maximally symmetric Lorenzian space; to give this phrase meaning, we first have to recap what diffeomorphisms are. Any continuous, isomorphic mapping of a manifold onto itself can be called a diffeomorphism. If a diffeomorphism leaves the metric, $g_{\mu\nu}$, invariant, it is called an isometry. Isometries are essentially the symmetries of a space. A general diffeomorphism can be written using a Lie-derivative $\mathcal{L}_\xi$ along a covector ξ_μ

$$g_{\mu\nu} \to g_{\mu\nu} + \mathcal{L}_\xi g_{\mu\nu} = g_{\mu\nu} + \nabla_\mu \xi_\nu + \nabla_\nu \xi_\mu \tag{2.1}$$

For the derivative to be an isometry, we require that the so-called Killing equation is fulfilled, meaning

$$\nabla_\mu \xi_\nu + \nabla_\nu \xi_\mu = 0. \tag{2.2}$$

Vectors ξ^μ that fulfil this equation are called Killing vectors. Each Killing vector will correspond to an isometry. A maximally symmetric space is a space with the maximum number of linearly independent Killing vectors. Knowing that the metric has $D(D+1)/2$ independent components, we see that there are at most $D(D+1)/2$ equations for independent Killing vectors. The group generated by the Killing vectors constitutes the maximally symmetric space, and it turns out that there are only three such spaces [18]. These are Minkowski space given by the Poincare group $\mathrm{ISO}(1, D)$, de Sitter space $\mathrm{SO}(1, D)$, and Anti-de Sitter space $\mathrm{SO}(2, D-1)$. All these three spaces are solutions to the sourceless[1] Einstein's equations

$$R_{\mu\nu} - \frac{1}{2} g_{\mu\nu}(R - 2\Lambda) = 0. \tag{2.3}$$

with a cosmological constant of $\Lambda = 0$, $\Lambda > 0$ and $\Lambda < 0$ respectively. $R_{\mu\nu}$ is the Ricci tensor and R is the Ricci scalar, both of which are defined using the metric $g_{\mu\nu}$. Anti-de Sitter space is the space relevant to our intents and purposes.

To better understand these D-dimensional spaces, we consider embeddings in $D+1$-dimensional space. The three maximally symmetric spaces in Euclidian space are $\mathbb{R}^D$, a sphere S^D, and a hyperboloid $\mathcal{H}^D$. In the same way, Anti-de Sitter space can be seen as an embedding of a hyperboloid in $\mathbb{R}^{1,D}$ that fulfils the constraint equation

$$-X_D^2 - X_0^2 + X_1^2 + X_2^2 + \ldots + X_{D-1}^2 = -L^2 \tag{2.4}$$

where L parameterises the curvature of the hyperboloid. We see the $\mathrm{SO}(2, D-1)$ symmetry manifest in (2.4).

To find a coordinate system for AdS_D space, the surface in (2.4) can be parameterised. Letting $D = d+2$ and $d > 0$, one parameterisation can be written as

$$\begin{aligned}
X_0 &= L\sqrt{1+\tan^2\rho}\sin\tau \\
X_1 &= L\tan\rho\cos\theta_1 \\
X_2 &= L\tan\rho\sin\theta_1\cos\theta_2 \\
&\vdots \\
X_{D-2} &= L\tan\rho\sin\theta_1\sin\theta_2\cdots\sin\theta_{d-1}\cos\theta_d \\
X_{D-1} &= L\tan\rho\sin\theta_1\sin\theta_2\cdots\sin\theta_{d-1}\sin\theta_d \\
X_D &= L\sqrt{1+\tan^2\rho}\cos\tau.
\end{aligned} \tag{2.5}$$

In this parametrisation there are the D coordinates, $\tau \in [0, 2\pi)$, $\rho \in [0, \pi/2)$, $\theta_i \in [0, \pi)$ for $i = 1, \ldots, d-1$, and lastly $\theta_d \in [0, 2\pi)$. Unrolling $\tau \in (-\infty, \infty)$

[1] Sourceless means we set the stress-energy tensor $T_{\mu\nu} = 0$.

gives the universal cover of AdS_D. The induced metric in these coordinates gives a topological understanding of AdS_D,

$$\begin{aligned} \mathrm{d}s^2 &= -\mathrm{d}X_0 - \mathrm{d}X_D + \sum_{i=1}^{D-1} \mathrm{d}X_i = \frac{L^2}{\cos^2\rho}\left(-\mathrm{d}\tau^2 + \mathrm{d}\rho^2 + \sin^2\rho\,\mathrm{d}\Omega_d^2\right) \sim \\ \mathrm{d}s^2_{\mathrm{teq}} &= \mathrm{d}\tau^2 + \mathrm{d}\rho^2 + \sin^2\rho\,\mathrm{d}\Omega_d^2, \end{aligned} \tag{2.6}$$

where $d\Omega_d$ is the metric on S^d. When only being interested in the topology of the metric, we can look at $\mathrm{d}s^2_{\mathrm{teq}}$, ignoring the factor in front. The metric describes a cylinder with longitudinal direction τ and radial direction of ρ with a boundary at $\pi/2$ as shown in figure 2.1. This boundary is called the *conformal boundary*.

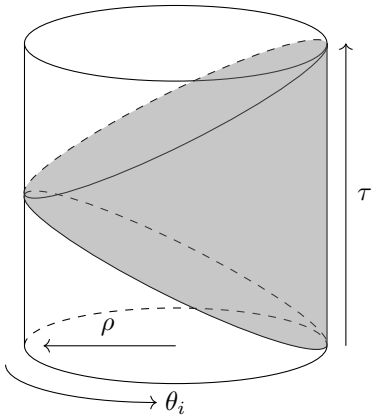

Figure 2.1: The topology of three-dimensional anti-de Sitter space illustrated as a cylinder with a conformal boundary at $\theta = 2\pi$. In higher dimensions, the radial coordinates θ_i parameterise S^d. The Poincaré patch (grey region) only covers a portion of AdS.

Yet another set of coordinates for AdS_D are the so-called *Poincaré coordinates*

$$\begin{aligned} X_0 &= \frac{L}{r}t \\ X_1 &= \frac{L}{r}x_1 \\ &\vdots \\ X_{D-2} &= \frac{L}{r}x_d \\ X_{D-1} &= \frac{1}{2r}\left(L^2 - r^2 + t^2 - \sum_i^d x_i^2\right) \\ X_D &= \frac{1}{2r}\left(L^2 + r^2 - t^2 + \sum_i^d x_i^2\right), \end{aligned} \tag{2.7}$$

where $r \in [0, \infty)$, $t \in (-\infty, \infty)$, and $x_i \in (-\infty, \infty)$, and the induced metric becomes

$$\mathrm{d}s^2 = \frac{L^2}{r^2}\left(-\mathrm{d}t^2 + \mathrm{d}r^2 + \mathrm{d}\vec{x}_d^2\right). \tag{2.8}$$

Unlike the previously mentioned cylindrical coordinates, the Poincaré coordinates do not give the universal cover for AdS_D. Relating the coordinates using (2.4), one can show that Poincaré coordinates cover the grey region seen in figure 2.1. This region is called the *Poincaré patch*. In Poincaré coordinates, the conformal boundary can be found at $r = 0$.

2.2 Correlation functions

To make any physical calculations in a quantum field theory, we need to evaluate n-point correlation functions. This comes most naturally in the path integral formulation. Start by looking at a scalar theory where we find the n-point correlation functions given as

$$\langle \phi(x_1) \dots \phi(x_n) \rangle = \frac{\int \mathcal{D}\phi \, \phi(x_1) \dots \phi(x_n) \, \mathrm{e}^{\mathrm{i}I[\phi]}}{\int \mathcal{D}\phi \mathrm{e}^{\mathrm{i}I[\phi]}}, \tag{2.9}$$

where $I[\phi]$ is the action of the theory. To evaluate this, a fictitious term is added in the exponent of the partition function as

$$Z[h] = \int \mathcal{D}\phi \, \mathrm{e}^{\mathrm{i}\int \mathrm{d}^4x \{\mathcal{L}[\phi] + h(x)\phi(x)\}}. \tag{2.10}$$

This is called the *generating functional* for the quantum field theory. The fictitious term, $h(x)$, is called a *source field*. Evaluating the n-point correlation functions is now easy with the help of the fictitious source $h(x)$. Using functional derivatives, we can bring down ϕ from the exponent, whereby we get the expression given in (2.9) from

$$\langle \phi(x_1) \dots \phi(x_n) \rangle = (-\mathrm{i})^n \frac{1}{Z[h]} \frac{\delta^n Z[h]}{\delta h(x_1) \dots \delta h(x_n)} \bigg|_{h=0}. \tag{2.11}$$

Making the above more general, we write all degrees of freedom of our theory as Φ. The partition function for any composite operator $\mathcal{O}$ of all fields in our quantum field theory is then written as

$$Z_{\mathcal{O}}[h] = \int \mathcal{D}\Phi \, \mathrm{e}^{\mathrm{i}\int \mathrm{d}^4x \left[\mathcal{L}[\Phi] + h(x)\mathcal{O}(x)\right]} \tag{2.12}$$

from which we can get the n-point correlation function analogously to before

$$\langle \mathcal{O}(x_1) \dots \mathcal{O}(x_n) \rangle = (-\mathrm{i})^n \frac{1}{Z_{\mathcal{O}}[h]} \frac{\delta^n Z_{\mathcal{O}}[h]}{\delta h(x_1) \dots \delta h(x_n)} \bigg|_{h=0}. \tag{2.13}$$

This discussion holds for both free and interacting theories. For free theories, the action is at most quadratic in the fields. This results in Gaussian integrals, which can be solved analytically. This is no longer the case in an interacting theory, however, which results in the need for converging approximate solutions such as perturbation theory.

2.3 The Holographic dictionary

We hope to construct a dictionary such that we can go back and forth between a theory for gravity and a dual QFT. Such a relation was given by Gubser, Klebanov, Polyakov [14], and Witten [15], which we will take for granted without going through any derivations. The most important result is the so-called GKWP rule, which relates the partition function of the dual theories,

$$Z_{\mathrm{QFT}}[h] = Z_{\mathrm{Grav}}[h]. \tag{2.14}$$

The contents of this equation call for an explanation. On the left-hand side, there is a QFT partition function analogous to the one discussed in the previous section. It is a generating functional for a dual QFT with a source $h(x)$ for some composite operator $\mathcal{O}$,

$$Z_{\mathrm{QFT}}[h] = \int \mathcal{D}\Phi \, \mathrm{e}^{\mathrm{i}\int \mathrm{d}^{d+1}x \, (\mathcal{L}[\Phi]+h(x)\mathcal{O}(x))}. \tag{2.15}$$

Now consider the partition function for the gravitational theory on the right-hand side of (2.14). The claim of the correspondence is that the fields inside the bulk are dual to the source in the boundary theory. This means that h will be the boundary value of some field inside the bulk. For the sake of clarity, consider only a scalar field in the bulk, which allows us to write

$$Z_{\mathrm{Grav}}[h] = \int^{\phi\to h} \mathcal{D}\phi \, \mathrm{e}^{\mathrm{i}S_{\mathrm{Grav}}[\phi]}. \tag{2.16}$$

Note that ϕ need not be a scalar field; it can be any dynamical field in the bulk, dual to a source with a corresponding observable in the QFT. The "$\phi \to h$" represents a boundary condition of ϕ at the conformal boundary, whereby we relate the boundary theory to the bulk. Knowing which bulk field corresponds to which source in the boundary theory can be tricky. A discussion on how to identify these correspondences is to come in section 2.3.1.

As mentioned in the introduction for a bulk theory in the classical limit, the corresponding boundary theory will be in the large N limit. The partition function, $Z_{\mathrm{Grav.}}$, can then be evaluated semi-classically using a saddle point approximation [17]

$$Z_{\mathrm{Grav}}[h] \approx \mathrm{e}^{\mathrm{i}S_{\mathrm{Grav}}[\phi^\star]}. \tag{2.17}$$

Here, $\phi^\star$ represents the ϕ that solves the equations of motion with the boundary condition that it is equal to $h(x)$ on the conformal boundary, $r = 0$. By (2.13), the GKWP rule then gives a simple formula for evaluating correlation functions in the large N limit for the boundary theory as

$$\langle \mathcal{O}(x_1) \dots \mathcal{O}(x_n) \rangle = \frac{\delta^n S_{\mathrm{Grav}}[\phi^\star]}{\delta h(x_1) \dots \delta h(x_n)}. \tag{2.18}$$

The entirety of the work done in this thesis will be in the classical limit. Therefore, this approximation and (2.14) will both be called the GKWP rule. The context of the calculations should make it clear which form is being used.

2.3.1 Bulk fields and sources

As mentioned, ϕ could be a scalar, vector, spinor, or any dynamical field in the bulk. In the classical limit, the solutions to ϕ are fully fixed by the equations of motion, and by setting the boundary conditions $\phi(r = 0) = h$ and forcing the field to be regular in the deep interior of the bulk, $r \to \infty$. What is relevant to our interests is the fact that the leading and subleading order behaviour in the radial direction of the solutions is fixed as

$$\phi = \phi_{(0)} r^{\Delta_{(0)}} + \phi_{(1)} r^{\Delta_{(1)}} + \text{h.o.t.} \tag{2.19}$$

We can make a remark that generally holds in standard quantisation; the leading behaviour, $\phi_{(0)}$, can be identified with the source in the boundary theory. The subleading $\phi_{(1)}$ can be identified with the expectation value of a composite operator in the boundary field theory, $\langle \mathcal{O} \rangle$. These roles can switch in alternative quantisation, with $\phi_{(1)}$ corresponding to the source and $\phi_{(0)}$ to the expectation value $\langle \mathcal{O} \rangle$. In our case, however, the aforementioned statement will always be true.

By construction, there is always a metric in the bulk, promoting it to be dynamic gives a corresponding source and composite operator in the boundary theory. The bulk action describing these dynamics is the Einstein-Hilbert action

$$S[g_{\mu\nu}] = \frac{1}{2\kappa^2} \int \mathrm{d}^{d+2}x \sqrt{-g}(R - 2\Lambda). \tag{2.20}$$

Coterminous examples of fields are the mentioned gauge fields or a scalar field giving the actions

$$S[\phi] + S[A_\mu] = \frac{1}{2} \int \mathrm{d}^{d+2}x \, \sqrt{-g} \left((\nabla\phi)^2 + (m\phi)^2 \right) - \frac{1}{4\alpha} \int \mathrm{d}^{d+2}x \sqrt{-g} F^2, \tag{2.21}$$

where $F_{\mu\nu}$ is the field strength tensor and ϕ a massive scalar field.

Knowing the action and knowing the bulk background, given a source h, enables the computation of correlation functions of operators $\langle \mathcal{O} \rangle$. To make use of the correspondence, we need to know what operators in the boundary theory the fields are dual to, which can be a difficult task. Luckily, the symmetries, or more specifically, the gauge symmetries of the theory, can shed some light on what sources the fields might be dual to. The gauge fields can be the Maxwell field, the metric, or any other non-abelian gauge field.

As a suitable example, let us see if any operator dual to a U(1) Maxwell field can be found. The action for this theory is the second term in (2.21). Considering the on-shell action indicated by the star of $S^\star$, we integrate by parts

$$S^\star[A_\mu] \propto \int_{\partial\mathcal{M}} \mathrm{d}^{d+1}x \, \sqrt{-\gamma} A_\nu n_\mu F^{\mu\nu}, \tag{2.22}$$

where n^μ is the outward-facing normal vector to the boundary, and γ is the determinant of the induced metric on the boundary, $\gamma_{\mu\nu} = g_{\mu\nu} - n_\mu n_\nu$. For the on-shell

action, only the boundary term is left as the bulk term is zero by the equations of motion. The action has to be invariant under gauge transformation of the field, so we make a gauge transformation to (2.22)

$$\begin{aligned}&\int_{\partial\mathcal{M}} \mathrm{d}^{d+1}x\,\sqrt{-\gamma}A_\nu n_\mu F^{\mu\nu} \to \int_{\partial\mathcal{M}} \mathrm{d}^{d+1}x\,\sqrt{-\gamma}\,(A_\nu+\nabla_\nu\chi)\,n_\mu F^{\mu\nu}\\ &=\int_{\partial\mathcal{M}} \mathrm{d}^{d+1}x\,\left(\sqrt{-\gamma}A_\nu n_\mu F^{\mu\nu}-\chi\nabla_\nu\left[\sqrt{-\gamma}n_\mu F^{\mu\nu}\right]\right)\end{aligned} \tag{2.23}$$

where the last equality follows after using integration by parts on the gauge term. We demand that the second term vanishes on the boundary such that the action is gauge invariant, resulting in a conserved vector on the boundary

$$j^\mu \sim \sqrt{-\gamma}n_\nu F^{\nu\mu}|_{\partial\mathcal{M}} \implies \nabla_\mu j^\mu = 0. \tag{2.24}$$

Here, we assert that *every bulk gauge symmetry has a corresponding global symmetry in the dual theory.* As an example consider a Maxwell field A_μ and the metric $g_{\mu\nu}$; these correspond to a current j^μ and a stress–energy tensor $\mathcal{T}^{\mu\nu}$ in the boundary [17]. Materials with a non-zero[2] Maxwell charge density $\rho = j^t$ are called *compressible.* A chemical potential, dual to the Maxwell field on the boundary $\mu = A_t|_{\partial\mathcal{M}} = \mathcal{A}_t$, generates this charge.

Matching up operators beyond their symmetries is often not possible, which is why it is important to understand that the bulk theory offers a complete description of the strongly coupled boundary theory. The properties of the dual operators, including their correlations, are determined entirely by the bulk fields. As such, referencing a QFT Lagrangian is the wrong approach to holography. Regardless, it can be comforting to reference what is familiar and digest the meaning of some fields in the gravity system. Considering a schematic Lagrangian for the QFT,

$$\mathcal{L} \sim \mathrm{tr}\left(F^2+(\nabla\Phi)^2+\mathrm{i}\bar{\Psi}\not{D}\Psi+\mathrm{i}\bar{\Psi}[\Phi,\Psi]-[\Phi,\Phi]^2\right), \tag{2.25}$$

a scalar field ϕ in the bulk might be dual to QFT operators such as $\mathrm{tr}F^2$, $\mathrm{tr}\Phi^2$, or $\mathrm{tr}\Psi\Psi$. Likewise, a fermion ψ in the bulk might be dual to a fermionic operator such as $\mathrm{tr}\Phi\Psi$.

2.3.2 Radial Dimension

The radial dimension is the cornerstone of the holographic principle. Here, we will briefly summarise the physical meaning of it and add the translation to our dictionary between the two theories. The short answer is that the radial direction in the bulk corresponds to the renormalisation group (RG) in the boundary. For context, we will start with a quick overview of *Wilsonian renormalisation.* This is followed by motivating why the radial direction in the gravity theory corresponds to RG. Holographic renormalisation as a whole is a vast subject that will not be covered beyond what is necessary for the topic at hand. The interested reader is referred to the literature [27–29].

[2]To be more precise, one can say that we require a continuously tunable charge density.

While the implementation of the renormalisation group varies in approach, it generally follows a structured process composed of three steps. We will restrict ourselves to a single field ϕ to ease notation. Suppose we have some quantum theory described by an action

$$I[\phi] \equiv \sum_{i=1}^{N} g_i \mathcal{O}_i[\phi] \tag{2.26}$$

where g_i are coupling constants corresponding to some composite operators $\mathcal{O}_i = \int \mathrm{d}^d x (\nabla\phi)^n \phi^m$. To impose a cutoff, the action is Wick rotated, after which $\phi(k)$, with k now being Euclidean, is restricted to $|k| < \Lambda$. We are left with the partition function up to a cutoff Λ,

$$Z_\Lambda = \int_\Lambda \mathcal{D}\phi \, \mathrm{e}^{-I_\mathrm{E}[\phi]}, \tag{2.27}$$

where I_E denotes the action being of Euclidean signature and all sources $h = 0$ have been set to zero for simplicity. This is the starting point for the renormalisation group method, which is attributed to Kenneth Wilson [30, 31]. A general implementation of the method entails the following three steps [3, 32, 33].

I: Subdivision of the field manifold

This initial step involves partitioning the field manifold. This can be done in many different ways but is typically done by splitting the high and low momentum degrees of freedom. Given $b < 1$, ϕ is split in two: $\phi(k)$ for $|k| < b\Lambda$ and $\hat{\phi}(k)$ for $b\Lambda < |k| < \Lambda$. The resulting partition function is then

$$Z(\Lambda) = \int_\Lambda \mathcal{D}\phi \mathcal{D}\hat{\phi} \, \mathrm{e}^{-I_\mathrm{E}[\phi+\hat{\phi}]}. \tag{2.28}$$

This method is known as *momentum shell integration*. It inherently introduces a cutoff dependence in the theory at intermediate stages.

II: RG step

The second step involves integrating over the short-range fluctuations, $\hat{\phi}$. Splitting (2.28) further gives

$$Z(\Lambda) = \int_{b\Lambda} \mathcal{D}\phi \, \mathrm{e}^{-I_\mathrm{E}[\phi]} \int_{[b\Lambda,\Lambda]} \mathcal{D}\hat{\phi} \, \mathrm{e}^{-\widetilde{I}_\mathrm{E}[\phi+\hat{\phi}]}. \tag{2.29}$$

Performing the integral over the fast degrees of freedom $\hat{\phi}(k)$ results in a series of operators of the slow degrees of freedom ϕ with some coefficients. These terms can be reabsorbed into $I_\mathrm{E}[\phi]$ giving an *effective action*, $I_\mathrm{Eff.}[\phi]$, where the coupling constants of the slow field operators are modified by the change from the fast degrees of freedom as $g_i' = g_i + \delta g_i$, giving

$$Z(\Lambda) = \int_{b\Lambda} \mathcal{D}\phi \, \mathrm{e}^{-I_\mathrm{Eff.}[\phi]}. \tag{2.30}$$

It is crucial to note that this integration process may lead to the emergence of new operators, which are absent in the initial bare action.

III: Rescaling

The final step rescales momentum, $k' = k/b$ (and therefore space $x' = bx$), such that the rescaled field ϕ' ranges the same momentum scale, $|k'| < \Lambda$, as the original field ϕ. When rescaling ϕ, it is done in such a way as to leave the leading operator in the action, often the kinetic term $\int \mathrm{d}^d x (\nabla\phi)^2$, invariant under the RG process. This results in a renormalised action, defined entirely by a set of modified coupling constants

$$I[\phi] = \sum_{i=1}^{N} g_i' \mathcal{O}_i[\phi]. \tag{2.31}$$

After performing the RG procedure above, the coupling constants $\{g_i\} = \mathbf{g}$ are mapped to a new set of constants $\{g_i'\} = \mathbf{g}'$. This mapping is tuned by b or equivalently by a new parameter $l = \ln b$. If l is taken to be infinitesimally small and the process is repeated, the change of the coupling constants can be written as a differential equation,

$$\beta(\mathbf{g}) = \lim_{l\to 0} \frac{\mathbf{g}' - \mathbf{g}}{l} \equiv \frac{\mathrm{d}\mathbf{g}}{\mathrm{d}l}. \tag{2.32}$$

These types of equations are called β-functions. To interpret β-functions, we can think of the coupling constants as flowing in parameter space[3], tracing out a path along l. The effective coupling constants are said to be *running* when they change, depending on what scale one looks at. All points in parameter space at which $\mathbf{g}$ is fixed under flow, meaning $\beta(\mathbf{g}) = 0$, are called *fixed points*. When a fixed point is reached, some operators might have vanished, getting absorbed in the effective action. These are called *irrelevant*, while operators that do contribute at specific scales are called *relevant*. Thus, given an energy scale, one can consider an *effective field theory* (EFT) comprised of only the relevant operators.

Following Refs. [17, 29, 34], we will now motivate why the radial direction can be interpreted as RG flow. Starting from a general partition function for a boundary QFT, we have

$$Z_{\mathrm{QFT}} = \int_{\Lambda} \mathcal{D}\phi\, \mathrm{e}^{\mathrm{i}I_{\mathrm{Eff.}}[\phi]} \qquad I_{\mathrm{Eff.}}[\phi] = I_0[\phi] + I_{\mathrm{UV}}[\phi]. \tag{2.33}$$

Here $I_0[\phi]$ is the microscopic action, and $I_{\mathrm{UV}}[\phi]$ contains all the degrees of freedom above Λ that have been integrated out, giving an effective action, $I_{\mathrm{Eff.}}$, at Λ. We hope to find this structure emerging from the radial direction in the bulk. Recalling the gravity partition function from (2.16), we now introduce a radial cutoff at $r = \epsilon$, giving

$$Z^{\epsilon}[\phi^{\epsilon}] = \int^{\phi\to\phi^{\epsilon}} \mathcal{D}\phi\, \mathrm{e}^{\mathrm{i}S[\phi]} \qquad S[\phi] = \int_{r>\epsilon} \mathrm{d}^{d+2}x\sqrt{-g}\,\mathcal{L} + S_{\mathrm{B}}[\phi,\epsilon]. \tag{2.34}$$

The new boundary condition is $\phi \to \phi^{\epsilon} \equiv \phi(\epsilon)$ for ϕ at the cutoff ϵ. Here, S_{B} is a boundary action at $r = \epsilon$, which can be interpreted as arising due to integrating the

[3]The coupling constants are the parameters that span the space of possible composite operators.

action at $r < \epsilon$. This is reminiscent of integrating the high degrees of freedom in RG giving I_{UV}. As we will shortly see, S_{B} will be translated to the dual I_{UV} [29].

Since the choice of ϵ is arbitrary, we have a requirement that the action does not change with ϵ,

$$\begin{aligned}\frac{\mathrm{d}}{\mathrm{d}\epsilon}S[\phi] &= \frac{\mathrm{d}}{\mathrm{d}\epsilon}\left[-\int_{\infty}^{\epsilon}\mathrm{d}r\int\mathrm{d}^{d+1}x\sqrt{-g}\,\mathcal{L}\right] + \frac{\partial}{\partial\epsilon}S_{\mathrm{B}}[\phi,\epsilon] + \int_{r=\epsilon}\mathrm{d}^{d+1}x\frac{\delta S}{\delta\phi}\partial_r\phi \\ &= \int_{r=\epsilon}\mathrm{d}^{d+1}x\left(\Pi\partial_r\phi - \sqrt{-g}\mathcal{L}\right) + \frac{\partial}{\partial\epsilon}S_{\mathrm{B}}[\phi,\epsilon] = 0 \\ &\implies \frac{\partial}{\partial\epsilon}S_{\mathrm{B}}[\phi,\epsilon] = -\int_{r=\epsilon}\mathrm{d}^{d+1}x\,\mathcal{H}.\end{aligned} \tag{2.35}$$

In the second equality, Π is introduced, denoting the canonical momentum along the radial direction. The canonical momentum, together with the Lagrangian density, constitutes a Legendre transform that results in the Hamiltonian density $\mathcal{H}$ for evolution in the radial direction. This is precisely the Hamilton-Jacobi equation but for ϵ-flow.

Consider the full bulk partition function (2.16) with the boundary condition of the field being equal to the source at $r = 0$. This can be constructed by connecting two path integrals at $r = \epsilon$ with (2.34) for $r > \epsilon$ and $Z^{\epsilon}_{\mathrm{UV}}$ for $r < \epsilon$,

$$Z[h] = \int\mathcal{D}\phi^{\epsilon}\,Z^{\epsilon}[\phi^{\epsilon}]Z^{\epsilon}_{\mathrm{UV}}[\phi^{\epsilon},h], \qquad Z^{\epsilon}_{\mathrm{UV}}[\phi^{\epsilon},h] \equiv \int\mathcal{D}\phi^{\epsilon}\,Z^{\epsilon}[\phi^{\epsilon}]\int_{\phi\to\phi^{\epsilon}}^{\phi\to h}\mathcal{D}\phi\,\mathrm{e}^{\mathrm{i}S[\phi]}. \tag{2.36}$$

To relate this to RG in the dual theory, we generalise the GKWP rule in (2.14) by claiming that the cutoff bulk partition function from (2.34) is equal to a QFT partition function at a cutoff $\Lambda \sim 1/\epsilon$,

$$Z^{\epsilon}[\phi^{\epsilon}] = \int_{\Lambda}\mathcal{D}\phi\,\mathrm{e}^{\mathrm{i}I_0[\phi]+\mathrm{i}\int\mathrm{d}^{d+1}x\,\phi^{\epsilon}(x)\mathcal{O}(x)}. \tag{2.37}$$

The expression $\Lambda \sim 1/\epsilon$ is not precise but merely a schematic device, as the actual relation between the cutoffs is unknown. Finding a relationship between the two would probably surmount to proving holographic duality [17]. Instead, we will conjecture the above, motivated by the resulting sensible physics.

Once again, using (2.14), we set (2.33) and (2.36) equal and insert our newfound correspondence for $Z^{\epsilon}[\phi^{\epsilon}]$. After some manipulation, we end up with

$$\mathrm{e}^{\mathrm{i}I_{\mathrm{UV}}[\mathcal{O}]} = \int\mathcal{D}\phi^{\epsilon}\,\mathrm{e}^{\mathrm{i}\int\mathrm{d}^{d+1}x\,\phi^{\epsilon}(x)\mathcal{O}(x)}Z^{\epsilon}_{\mathrm{UV}}[\phi^{\epsilon},h], \tag{2.38}$$

which can be further simplified in the semi-classical limit,

$$I_{\mathrm{UV}}[\mathcal{O}] = \int\mathrm{d}^{d+1}x\,\phi^{\epsilon}_{\star}(x)\mathcal{O}(x) + S_{\mathrm{B}}[\phi^{\epsilon}_{\star},\epsilon], \tag{2.39}$$

where $S_{\mathrm{B}}[\phi^{\epsilon}_{\star},\epsilon]$ comes out of $Z^{\epsilon}_{\mathrm{UV}}[\phi^{\epsilon}]$. The stars indicate the on-shell solutions. Looking at the dependence of the right- and left-hand side of (2.39), we further see two corollary relations

$$\frac{\delta I_{\mathrm{UV}}}{\delta\mathcal{O}} = \phi^{\epsilon}_{\star} \qquad \frac{\delta S_{\mathrm{B}}}{\delta\phi^{\epsilon}_{\star}} = -\mathcal{O}. \tag{2.40}$$

Finally, all that is left to do is exactly what was done in (2.35), namely to take a derivative with respect to ϵ to find flow equations for I_{UV}. The resulting flow equation for I_{UV} is the same as for S_{B},

$$\begin{aligned}\frac{\mathrm{d}}{\mathrm{d}\epsilon}I_{\mathrm{UV}}[\mathcal{O}] &= \frac{\partial I_{\mathrm{UV}}}{\partial\epsilon} + \int_{r=\epsilon}\mathrm{d}^{d+1}x\,\frac{\delta I_{\mathrm{UV}}}{\delta\mathcal{O}}\frac{\partial\mathcal{O}}{\partial\epsilon} \\ &= \int_{r=\epsilon}\mathrm{d}^{d+1}x\left(\frac{\partial\phi_\star^\epsilon}{\partial\epsilon}\mathcal{O} + \phi_\star^\epsilon\frac{\partial\mathcal{O}}{\partial\epsilon}\right) + \frac{\partial S_{\mathrm{B}}}{\partial\epsilon} + \int_{r=\epsilon}\mathrm{d}^{d+1}x\,\frac{\delta S_{\mathrm{B}}}{\delta\phi_\star^\epsilon}\frac{\partial\phi_\star^\epsilon}{\partial\epsilon} \\ \implies \frac{\partial}{\partial\epsilon}I_{\mathrm{UV}}[\mathcal{O}] &= \frac{\partial}{\partial\epsilon}S_{\mathrm{B}} = -\int_{r=\epsilon}\mathrm{d}^{d+1}x\,\mathcal{H}.\end{aligned} \tag{2.41}$$

The cutoff ϵ generates RG flow in the dual QFT.

One can expand $I_{\mathrm{UV}}[\mathcal{O}]$ in a series of operators, $\mathcal{O}$, as

$$I_{\mathrm{UV}}[\mathcal{O}] = \sum_n\int\mathrm{d}^{d+1}x\sqrt{-\gamma}\lambda_n(x,\Lambda)\mathcal{O}(x)^n, \tag{2.42}$$

where the λ_n are the coupling constants in the effective theory. All β-functions for all λ_n can be constructed by inserting this expansion into (2.41), [17]. Thus, we have good reason to believe that the assertion that (2.37) holds for some $\Lambda \sim 1/\epsilon$. While we cannot know the exact relation, we can go to extremes in the radial direction and thereby flow from the UV at $r \to 0$ to IR fixed points at $r \to r_+$ where r_+ can be ∞ or, which will be the topic of the next section, the horizon of a black hole.

2.3.3 Turning on a temperature

In 1916, Karl Schwarzschild presented the second-ever solution to Einstein's equations [35], giving a general metric symmetric under time translations and rotations. This was dubbed the Schwarzschild solution. A rather peculiar result of the Schwarzschild solution was that it, by construction, predicted black holes. It was later discovered that black holes exhibit thermodynamic properties [36–38]. Given the nature of the AdS/CFT correspondence, it may then seem enticing to introduce a black hole inside the AdS bulk with the hopes of the thermodynamic properties of a black hole carrying over to the QFT. As it turns out, holographic duality fulfils our wishes once more, whereby the thermodynamics of a black hole "project" onto the boundary theory. The Hawking temperature and other thermodynamic properties, such as the Bekenstein-Hawking entropy of the black hole, are inherited by the boundary theory, giving rise to temperature, entropy, and more. This follows directly from a thermodynamic field theory treatment of the GKWP rule [17].

We begin by modifying the flat AdS metric by introducing a black hole in the bulk

$$\mathrm{d}s^2 = \frac{L^2}{r^2}\left(f(r)\mathrm{d}\tau^2 + \frac{1}{f(r)}\mathrm{d}r^2 + \mathrm{d}\Sigma^2\right). \tag{2.43}$$

Here, we have made a Wick rotation, $t \to \mathrm{i}\tau$, going to Euclidean signature in the metric. Furthermore, the emblackening factor for the black hole $f(r)$ has been

introduced. In the tried and true Schwarzschild solution, $\mathrm{d}\Sigma$ gives the geometry for a spherical horizon. However, this does not have to be the case for an AdS black hole where the horizon can be spherical, flat, or hyperbolic [18]. The simplest case is that of a flat horizon where $\mathrm{d}\Sigma^2 = \sum_{i=1}^{d} \mathrm{d}x_i^2 \equiv \mathrm{d}x^2$. This will also be the one we choose in our bottom-up approach as it is the most suitable one for calculations. While this does mean that the black hole is in actuality a black plane, we will insist on calling it a black hole, as is usual.

It is worth mentioning that introducing the metric (2.43) surmounts the theory having a sense of scale, thereby breaking the conformal symmetry. One might worry as this was one of the ingredients in the AdS/CFT correspondence. Alas, this disruption is necessary as condensed matter systems are inherently scale-dependent. Near the conformal boundary, the metric reverts to the form given by (2.8), yielding a CFT in the UV region. Consequently, the dual field theory can be seen as transitioning from a scale-invariant CFT in the UV to a scale-dependent theory in the IR, which corresponds to condensed matter theory (CMT).

For the horizon to be black, we have $f(r_+) = 0$ where r_+ is the horizon radius. Expanding f around r_+ to first order and ignoring higher order terms allows us to write the metric as

$$\mathrm{d}s^2 = \frac{L^2}{r_+^2}\left(|f'(r_+)|(r_+ - r)\mathrm{d}\tau^2 + \frac{1}{|f'(r_+)|(r_+ - r)}\mathrm{d}r^2 + \mathrm{d}x^2\right). \tag{2.44}$$

The behaviour of this metric is elucidated after the coordinate transformation

$$r = r_+ - \frac{r_+^2|f'(r_+)|}{4L^2}\rho^2, \quad \tau = \frac{2}{|f'(r_+)|}\varphi \implies \mathrm{d}s^2 = \rho_0^2\mathrm{d}\varphi^2 + \mathrm{d}\rho^2 + \frac{L^2}{r_+^2}\mathrm{d}x^2. \tag{2.45}$$

This is precisely the metric for cylindrical coordinates in flat space. To avoid a conical singularity at the horizon $\rho = 0$, the identification $\varphi \sim \varphi + 2\pi$ must hold [17]. This gives the identification $\tau \sim \tau + 4\pi/|f'(r_+)|$ for the imaginary time.

To relate this result to a temperature, we backtrack and consider a thermodynamic partition function for a quantum mechanical system. The partition function can be written as

$$Z = \mathrm{Tr}[\mathrm{e}^{-\beta\hat{H}}] = \sum_{\lambda}\langle\lambda|\mathrm{e}^{-\beta\hat{H}}|\lambda\rangle. \tag{2.46}$$

The temperature is given by the thermodynamic beta $\beta = 1/T$. Thinking of this as evolution in imaginary time, there is a striking similarity between the partition function and the transition amplitude for a system from ϕ_i to ϕ_f in t_f time [16]. We write such a transition as a path integral

$$\langle\phi_f, t_f|\phi_0, 0\rangle = \int \mathcal{D}\phi(t)\,\mathrm{e}^{\mathrm{i}\int_0^{t_f}\mathrm{d}tL[\phi(t)]}. \tag{2.47}$$

Starting from the transition, we wish to arrive at the thermodynamic partition function, which we do by firstly summing over all transitions where $\phi_i = \phi_f$ in time

t_f. This is followed by substituting $t_f \to -\mathrm{i}\beta$. We also Wick rotate $t \to -\mathrm{i}\tau$ the time dummy variable, as to make sense of the integral in the exponent. In total, this manipulation results in

$$Z = \int_{\mathrm{PBC}} \mathcal{D}\phi(\tau)\, \mathrm{e}^{-\int_0^\beta \mathrm{d}t L_{\mathrm{E}}[\phi(\tau)]}, \tag{2.48}$$

where L_E denotes the Euclidean Lagrangian after Wick rotation. By periodic boundary conditions, we mean that we are integrating over all paths such that the final state and initial states are the same, $\phi(\tau = 0) = \phi(\tau = \beta)$. Letting τ run from $-\infty$ to ∞, we thus have periodic boundary conditions with a periodicity of β, allowing us to make the identification $\tau \sim \tau + \beta = \tau + 1/T$.

Returning to the identification in τ that we found from the geometry at the Euclidian horizon, we can set it equal to the β from above, arriving at the Hawking temperature of the black hole

$$T = \frac{|f'(r_+)|}{4\pi}. \tag{2.49}$$

Beyond temperature, other thermodynamical properties such as entropy or free energy can be obtained in a similar manner [18], although, for this thesis, the temperature will suffice.

2.4 Example: Massive scalar field

To elucidate the discussion around the dictionary above, the most basic holographic model, the scalar field, will be done step by step. Despite its simplicity, this example contains general lessons for all holographic calculations and can thus be considered the canonical example [17] for holographic calculations. Begin by considering a free massive scalar field in an AdS_{d+2} bulk with the familiar action

$$S[\phi] = -\int \mathrm{d}^{d+2}x \sqrt{-g} \left(\frac{1}{2}(\partial\phi)^2 + \frac{m^2}{2}\phi^2 \right). \tag{2.50}$$

In this simple case, we take the field to be minimally coupled, meaning the scalar field does not couple with the metric, g. Furthermore, the system is considered at zero temperature, resulting in the vacuum AdS_{d+2} solution from section 2.1. Using Poincaré coordinates, the metric is

$$\mathrm{d}s^2 = \frac{L^2}{r^2}\left(-\mathrm{d}t^2 + \mathrm{d}r^2 + \mathrm{d}\vec{x}_d^2\right), \tag{2.51}$$

where r is the radial dimension with the conformal boundary located at $r = 0$. Henceforth, the vector notation and d subscript will be dropped for $\vec{x}_d$. By varying the action, the stationary action principle gives the equations of motion as

$$(\nabla^2 - m^2)\phi = \frac{1}{\sqrt{-g}}\partial_\mu\left(\sqrt{-g}g^{\mu\nu}\partial_\nu\phi\right) - m^2\phi = 0. \tag{2.52}$$

The boundary terms are ignored for now but as was seen in section 2.3.1 they will play an important part for dual boundary sources and operators.

We can solve the equation of motion by making a plane wave ansatz. Choosing the coordinate system such that k is along x, the ansatz for the scalar field reads

$$\phi = \phi(r) \exp\left(-\mathrm{i}\omega t + \mathrm{i}kx\right). \tag{2.53}$$

The ansatz in the equations of motion together with the metric from (2.51) gives $\sqrt{-g} = \left(\frac{L}{r}\right)^{d+2}$ and the equation of motion becomes

$$\phi'' - \frac{d}{r}\phi' + \left(\omega^2 - k^2 - \frac{m^2 L^2}{r^2}\right)\phi = 0, \tag{2.54}$$

where $\phi' \equiv \partial_r \phi(r)$. Our interest ultimately lies in the asymptotic behaviour of ϕ in the UV limit, $r \to 0$. We can investigate phi in this regime by considering the leading order in a Laurent expansion in $\phi(r)$,

$$\phi(r) = \phi_{(\Delta)} r^{\Delta} + \text{h.o.t.} \tag{2.55}$$

When substituted into (2.54), this gives

$$(\Delta^2 - (d+1)\Delta - m^2 L^2) r^{\Delta - 2} + \text{h.o.t} = 0. \tag{2.56}$$

For the asymptotic behaviour, Δ is solved in the limit of $r \to 0$, giving

$$\Delta_{\pm} = \frac{d+1}{2} \pm \sqrt{\left(\frac{d+1}{2}\right)^2 + m^2 L^2}, \tag{2.57}$$

which lets us write (2.55) as

$$\phi(r) = \phi_{(0)} r^{\Delta_-} + \phi_{(1)} r^{\Delta_+} + \dots. \tag{2.58}$$

To use the GKWP rule, we would like to rewrite the on-shell action and simplify it slightly. Integrating the action, (2.50), by parts, we find

$$S[\phi] = \frac{1}{2}\int_{r>\epsilon} \mathrm{d}^{d+2}x\, \phi\sqrt{-g}\left(\nabla^2\phi - m^2\right)\phi - \frac{1}{2}\int_{r=\epsilon} \mathrm{d}^{d+1}x\, \sqrt{-\gamma}\phi n_\mu \partial^\mu \phi \tag{2.59}$$

where the boundary term results from using Stokes' theorem. Here, $n_\mu = -\frac{r}{L}\delta_{\mu r}$ is the outward-facing normal to the boundary and $\gamma_{\mu\nu} = g_{\mu\nu} - n_\mu n_\nu$ is the induced metric on the boundary. Letting the action be on-shell, the bulk integral is immediately zero due to the equations of motion. The boundary term, however, diverges, as we will see shortly, so it has to be regulated. Regularisation is done by introducing a cutoff at ϵ. Using the asymptotic solution for ϕ from (2.55) we find that

$$S^\star[\phi] = \frac{1}{2}\int_{r=\epsilon} \mathrm{d}^{d+1}x\, \left[\phi_{(0)}^2 \Delta_- r^{2\Delta_- - d - 1} + \phi_{(1)}^2 \Delta_+ r^{2\Delta_+ - d - 1} + (d+1)\phi_{(0)}\phi_{(1)}\right]. \tag{2.60}$$

Here we allow ourselves the liberty of absorbing factors of L into $\phi_{(0)}$ and $\phi_{(1)}$ as $\phi_{(1,2)} \to \phi_{(1,2)}/L^{d/2}$. With the $\Delta_\pm$ found in (2.58), the $\phi_{(1)}$-term vanishes as $\epsilon \to 0$,

while the $\phi_{(0)}$-term diverges. To counteract this divergence we modify the action by introducing a counterterm

$$\begin{aligned} S \to S + S_{\text{c.t.}} &= S - \frac{\Delta_-}{2L}\int_{r=\epsilon} \mathrm{d}^{d+1}x\sqrt{-\gamma}\phi^2 \\ \implies S^\star &= \frac{1}{2}\int_{r=\epsilon} \mathrm{d}^{d+1}x\,(2\Delta_+ - d - 1)\,\phi_{(0)}\phi_{(1)} + \mathcal{O}(\epsilon), \end{aligned} \tag{2.61}$$

which gives a finite on-shell action on the boundary. The counterterm does not alter the equations of motion in the bulk or the asymptotic behaviour of the field, since it is defined only using boundary data [17]. This divergence exemplifies the broader association between the vicinity of the boundary region in the bulk and the UV behaviour of the corresponding dual quantum field theory, as discussed in section 2.3.2. The leading term, $\phi_{(0)}$, can be identified with the source in the boundary theory h, allowing for the GKWP rule to be used,

$$\langle \mathcal{O} \rangle = \frac{\delta S^\star[\phi]}{\delta h} = \frac{2\Delta_+ - d - 1}{2}\frac{\delta}{\delta\phi_{(0)}}\left(\phi_{(0)}\phi_{(1)}\right). \tag{2.62}$$

This expression should give us pause; note that ϕ is fixed throughout the entire bulk by the equations of motion when $\phi_{(0)}$ is set by the boundary condition, provided that regularity is enforced.

With this in mind $\phi_{(0)}$ and $\phi_{(1)}$ have to be related by a linear matrix equation. The functional derivative in (2.62) then gives

$$\phi_{(1)} = \mathcal{M}\phi_{(0)} \implies \frac{\delta}{\delta\phi_{(0)}}\left(\phi_{(1)}\phi_{(0)}\right) = \mathcal{M}\frac{\delta\phi_{(0)}}{\delta\phi_{(0)}}\phi_{(0)} + \phi_{(1)} = 2\phi_{(1)}, \tag{2.63}$$

which results in an explicit expression for the correlation function of the dual operator in terms of the bulk field ϕ as

$$\langle \mathcal{O} \rangle = (\Delta_+ - \Delta_-)\,\phi_{(1)}. \tag{2.64}$$

Alone, this expression holds no value; to extract what is interesting, we must explicitly solve the equations of motions inside the bulk. In most instances, the solutions will have to be evaluated numerically, as will be the case for the models to come. As for (2.54), the simplicity of the equations allows for analytical solutions using Bessel functions. To find these solutions, a change of variables is due,

$$\phi(r) = r^{\frac{d+1}{2}}y(r), \qquad x = r\sqrt{k^2 - \omega^2}. \tag{2.65}$$

In this new set of variables (2.54) becomes the modified Bessel differential equation

$$x^2y''(x) + xy'(x) - (x^2 + \nu^2)y(x) = 0, \qquad 2\nu = \Delta_+ - \Delta_-. \tag{2.66}$$

When restricted to spacelike momenta[4], $k^2 - \omega^2 > 0$, the general solution to this equation is

$$y(x) = AI_\nu + BY_\nu, \tag{2.67}$$

[4]This restriction results in the retarded correlation functions. With timelike momenta one arrives at advanced correlation functions given by Hankel functions [18].

where I_ν is the modified Bessel functions of the first kind and Y_ν is the modified Bessel function of the second kind

$$I_\nu(x) = \sum_{n=0}^{\infty} \frac{1}{n!\Gamma(n+\nu+1)} \left(\frac{x}{2}\right)^{2n+\nu}, \qquad K_\nu(x) = \frac{\pi}{2} \frac{I_{-\nu}(x) - I_\nu(x)}{\sin(\nu\pi)}. \tag{2.68}$$

Enforcing $\phi(r \to \infty)$ to be regular tells us that $A = 0$. The field ϕ has now been determined up to a normalisation B as

$$\phi \propto r^{\frac{d+1}{2}} Y_\nu \left(r\sqrt{k^2 - \omega^2}\right) \mathrm{e}^{\mathrm{i}kx - \mathrm{i}\omega t}. \tag{2.69}$$

The coefficients to r^{Δ_-} and r^{Δ_+} can be identified with $\phi_{(0)}$ and $\phi_{(1)}$ by looking at the expansion of K_ν. Ignoring all normalisation factors that drop in two-point correlators, we find that

$$\phi_{(0)} \propto \frac{2^\nu}{\Gamma(1-\nu)} (k^2 - \omega^2)^{-\frac{\nu}{2}}, \qquad \phi_{(1)} \propto \frac{1}{2^\nu \Gamma(1-\nu)} (k^2 - \omega^2)^{\frac{\nu}{2}}. \tag{2.70}$$

Using this result together with (2.64) and (2.13), we can construct the retarded Green's function

$$G^{\mathrm{R}}_{\mathcal{O}\mathcal{O}}(\omega, k) = \frac{\langle \mathcal{O} \rangle}{h} = \frac{2\nu\phi_{(1)}}{\phi_{(0)}} = -\frac{\nu}{2^{2\nu-1}} \frac{\Gamma(1-\nu)}{\Gamma(1+\nu)} (k^2 - \omega^2)^\nu. \tag{2.71}$$

The scalar field in itself will be of little interest to the subject matter of this thesis. Nevertheless, there are ample lessons to be learned from this simple example. Starting from an action, we found correlation functions for $\mathcal{O}$ in the boundary theory solely by solving classical equations of motion in the bulk. After formulating a bulk action dual to a strongly correlated metal, we will make an analogous calculation but instead arrive at correlation functions for the boundary currents.

3. Ersatz Fermi-liquids

This chapter will mainly be a summary and review of two papers. First, we summarise and review Ref. [23], which presents a general formulation of Luttinger's theorem, which forms the foundation of the main crux of this thesis. Thereafter, we review and summarise Ref. [21], which presents a holographic description of an effective field theory, building upon the framework established when discussing Luttinger's theorem. Throughout this chapter, the language from Wilsonian renormalisation presented in section 2.3.2 will be used extensively.

The microscopic degrees of freedom in a material exhibit symmetries given by the system at hand. A simple example of such a microscopic symmetry is that of a lattice system. Such a system exhibits the same physics under translation as long as one keeps to the lattice. Whatever the symmetry of the UV might be, we label its group by G_{UV}. Under Wilsonian RG flow, the emergent IR effective theory can exhibit a larger symmetry. Again, we give this emergent symmetry group in the IR the general label G_{IR}. Predicting the emergence of G_{IR} from G_{UV} can often be an impossibly difficult task [23]. There are, however, some theorems which relate UV properties to the emergent IR properties [39–41]. One such theorem is Luttinger's theorem [22, 42], which will provide an important framework for the remainder of this thesis. Specifically, it is relevant for metals. As it is the focal point of this thesis, we should be specific about what a metal is and thus make a very general definition.

Definition of a metal

Consider a QFT with continuous translation symmetry and U(1) symmetry with a non-zero charge density ($\rho \neq 0$). This QFT will RG flow to an effective field theory in the IR. We define any such EFT as a metal.

Another important concept for characterising metals will be the *'t Hooft anomaly*. A sufficient definition for the 't Hooft anomaly is as follows: given an emergent symmetry G_{IR}, a corresponding conservation law exists by Noether's theorem. When the IR theory is coupled to a background gauge field, the symmetry is broken. The 't Hooft anomaly precisely encodes how this symmetry is broken when the theory is coupled to a gauge field.

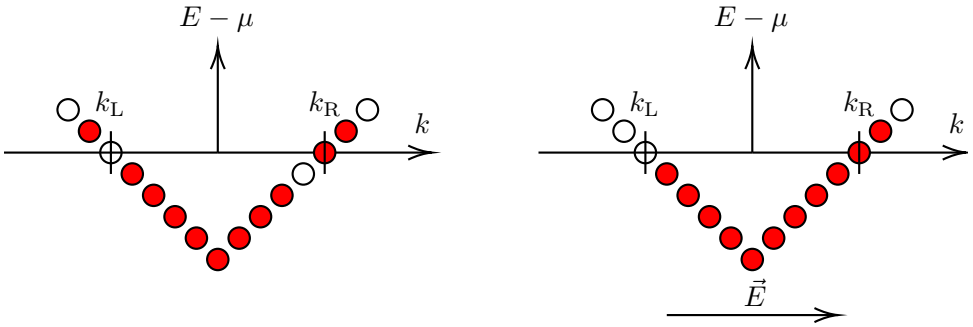

Figure 3.1: Schematic for the Fermi surface and the chiral behaviour of a low-energy Fermi gas in one dimension with and without a background electric field pointing to the right. The Fermi surface is located at the points k_{L} and k_{R}. The energy is shifted down by the chemical potential μ. Excitations accumulate at the right Fermi point when a right-facing electric field is present.

3.1 Luttinger's theorem

Imagine a translation[5] invariant system of spinless fermions in one spatial dimension. We will refer to this system as a Luttinger liquid. The symmetries of the microscopic theory are translations $\mathbb{T}$ and a U(1) symmetry generated by the conserved total charge $\hat{Q}$. Thus, we denote $G_{\mathrm{UV}} = \mathbb{R} \times \mathrm{U}(1)$, where $\mathbb{R}$ is the one-dimensional translation symmetry. Under RG, this flows to some emergent internal symmetries in the IR, resulting in an emergent symmetry group, G_{IR}.

Regardless of whether interactions in the Luttinger liquid are strong, weak, or none, the arguments for an emergent symmetry of the IR hold. The non-interacting system is, however, especially intuitive, and as such, we can use it to picture the system. In the case of no interactions, we have to accommodate a number of fermions. These fill the lowest energy states. Low-energy excitations then live near two points in momentum space as the space is one-dimensional. Denoting these two points as k_{L} and k_{R}, they constitute the Fermi surface. A schematic can be seen on the left in figure 3.1.

The IR theory has a chirality; right- and left-moving excitations are separately conserved, giving the emergent symmetry $G_{\mathrm{IR}} = \mathrm{U}(1)_{\mathrm{L}} \times \mathrm{U}(1)_{\mathrm{R}}$. Turning on a background electrical field, the G_{IR} acquires an axial anomaly as right and left movers are no longer separately conserved. The axial anomaly here is an example of an 't Hooft anomaly. Returning to the simple non-interaction example, this can be thought of as the charges accumulating at k_{R} as the electric field exerts a rightward force. This is depicted in the right schematic in figure 3.1. The continuity equations for G_{IR} thus become anomalous when coupled to an electric field ,

$$\partial_\mu j_R^\mu = \frac{E}{2\pi}, \qquad \partial_\mu j_L^\mu = -\frac{E}{2\pi}, \tag{3.1}$$

[5]When considering metals and the like, one often takes the microscopic theory to be on a lattice, thereby giving lattice translations $\mathbb{Z}$. In our case, it makes no difference if the translations are continuous or on a lattice. Thus, we assume the more general case.

where μ admits t and x. Now consider how G_{UV} maps to G_{IR} under RG. Translations are generated by the momentum and the U(1) symmetry is generated by the total charge, allowing us to make a mapping between the UV and IR as

$$\hat{Q} \sim \hat{N}_{\mathrm{L}} + \hat{N}_{\mathrm{R}}, \qquad \mathbb{T} \sim \exp\left(-\mathrm{i}[\hat{N}_{\mathrm{L}} k_{\mathrm{L}} + \hat{N}_{\mathrm{R}} k_{\mathrm{R}}]\right), \tag{3.2}$$

where $\hat{N}_{\mathrm{L}}$ and $\hat{N}_{\mathrm{R}}$ are the number operators for left and right movers, respectively. Consider the one spatial dimension of the Luttinger liquid closing on a circle. Furthermore, consider turning on a magnetic flux, Φ. The flux threads the circle from 0 up to 2π flux after t_f time. By Faraday's law, the Luttinger liquid then couples to a rightward electric field as

$$\partial_t \Phi = 2\pi R E, \tag{3.3}$$

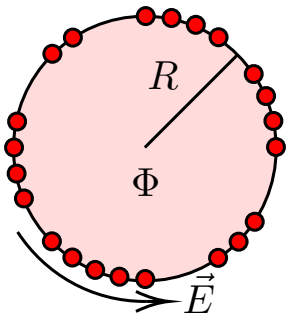

Figure 3.2: A schematic of a Luttinger liquid placed on a circle of radius R with an induced electric field E by threading a magnetic flux Φ.

where R is the radius of the circle. The set-up is depicted in figure 3.2. This results in the anomalous continuity equations (3.1). By integrating both equations over the circle, the spacial current term vanishes, leaving

$$\begin{aligned} -\partial_t \hat{N}_{\mathrm{L}} = -ER \implies \Delta \hat{N}_{\mathrm{L}} = -1, \\ -\partial_t \hat{N}_{\mathrm{R}} = ER \implies \Delta \hat{N}_{\mathrm{R}} = +1, \end{aligned} \tag{3.4}$$

where $\Delta \hat{N}_{\mathrm{L}}$ and $\Delta \hat{N}_{\mathrm{R}}$ is the shift in left and right moving charges after t_f time. Stated plainly, the 2π-flux threading process has exchanged one left-mover with one right-mover. The effect on (3.2) after flux threading is that the translation changes as $\mathbb{T} \to \mathbb{T} \exp\left(\mathrm{i}[k_{\mathrm{R}} - k_{\mathrm{L}}]\right)$.

If we now consider the microscopic theory with the charge density ρ, we see that the same process shifts the momentum

$$\partial_t p = 2\pi R \rho E \implies \Delta p = 2\pi \rho, \tag{3.5}$$

where the change in momentum is after t_f time as before. The change in $\mathbb{T}$ is given by the change in momentum p, and the microscopic theory then becomes $\mathbb{T} \to \mathbb{T} \exp\left(\mathrm{i}2\pi\rho\right)$. The change of $\mathbb{T}$ due to flux threading in the two evaluations has to agree, allowing us to equate the exponents relating the microscopic charge density to the Fermi surface

$$\frac{k_{\mathrm{R}} - k_{\mathrm{L}}}{2\pi} = \rho. \tag{3.6}$$

This relation is called Luttinger's theorem, which was first proven in Ref. [22] using perturbative techniques in Fermi liquid theory. Here, however, it was derived for the Luttinger liquid using only more general arguments from the symmetries in the UV and IR, how the UV maps to the IR, and the anomaly of the theory. With this, we conclude our discussion of the one-dimensional metal.

3.1.1 Two spatial dimensions

As we transition from the $1+1$-dimensional metal to the $2+1$-dimensional system, the derivation of Luttinger's theorem using the same foundational arguments becomes more complex. Readers interested in delving deeper into the intricacies are referred to Ref. [23]. Here, we will instead provide a succinct overview to motivate the formulation of Luttinger's theorem in two spatial dimensions.

For the Luttinger liquid, the IR emergent symmetry group is $G_{\text{IR}} = \text{U}(1)_{\text{L}} \times \text{U}(1)_{\text{R}}$, given by the conservation of charge at the two Fermi surface points separately. This result turns out to hold in any dimension; the charge at every point on the Fermi surface is conserved separately [43]. To be more precise, on a one-dimensional Fermi surface, there can no longer be a charge at every point. Instead, there is a charge density at every point that is separately conserved. We let this charge density be denoted by $\hat{n}(\theta)$, where θ parameterises the Fermi surface, as shown in figure 3.3. The total charge is then found by integrating the distribution over the whole Fermi surface, $\hat{Q} = \int \mathrm{d}\theta\, \hat{n}(\theta)$. A general element of G_{IR} can thus be identified as

$$\exp\left(-\mathrm{i}\int \mathrm{d}\theta f(\theta)\hat{n}(\theta)\right), \tag{3.7}$$

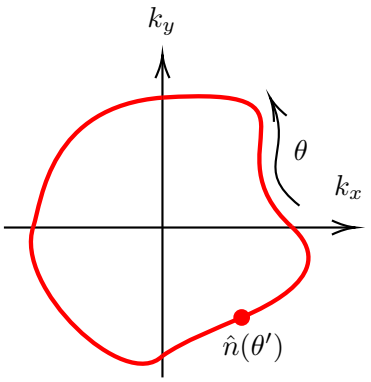

Figure 3.3: A general Fermi surface for metal in two spacial dimensions parameterised by θ.

where $f(\theta)$ has to be a smooth function. Since the total charge $\hat{Q}$ is quantised, admitting integer values, we can make the identification $f(\theta) \sim f(\theta) + 2\pi$, meaning $f(\theta)$ maps from a circle to a circle, or equivalently, from S^1 to U(1). We conclude that G_{IR} is isomorphic to smooth functions that map the S^1 to U(1). Groups mapping S^1 to some group G are called *"loop groups"* of G [44]. Following Ref. [21, 23] we use the notation $G_{\text{IR}} = \text{LU}(1)$, where LU(1) is the loop group of U(1). Furthermore, theories with this emergent LU(1) symmetry are defined as *"ersatz Fermi liquids"* (EFL).

Having identified the emergent symmetry, the mapping from the G_{UV} to the G_{IR}, $\varphi : \mathbb{R}^2 \times \text{U}(1) \to \text{LU}(1)$, is next. We have already seen the mapping of U(1) as the integral over the charge distribution. The translation operator mapping is trivial when following the logic of the Luttinger liquid. Denoting the Fermi surface components parameterised by θ in momentum space as $k_i(\theta)$ with $i = x, y$, the mapping can be identified as

$$\hat{Q} \sim \int \mathrm{d}\theta\, \hat{n}(\theta), \qquad \mathbb{T}_i \sim \exp\left(-\mathrm{i}\int \mathrm{d}\theta\, k_i(\theta)\hat{n}(\theta)\right) \tag{3.8}$$

where $\mathbb{T}_i$ are the translation operators in $i = x, y$ directions.

The final piece missing from Luttinger's theorem is the 't Hooft anomaly for the LU(1) symmetry. We can think of the theory coupling to a LU(1) gauge field as

inducing a current on the Fermi surface, causing $\hat{n}(\theta)$ to not be conserved. Here, we must clarify the meaning of a LU(1) gauge field. Since LU(1) symmetry roughly gives a conserved charge for each θ, we can think of it as a U(1) charge at each point on S^1. Each θ would then give a separate U(1) gauge field, $A_\mu(\theta)$, with the gauge transformation

$$A_\mu(\theta) \to A_\mu(\theta) + \partial_\mu \lambda(\theta). \tag{3.9}$$

As has already been mentioned, our arguments do not care about interactions and are general for any compressible theory. As it stands, the gauge field is unable to explain certain effects in Fermi liquid theory associated with moving quasiparticles around the Fermi surface. Describing these effects requires an additional component, A_θ. We assume A_θ remains for non-Fermi liquids [21]. The gauge field can thus then be said to live on a manifold $M \times S^1$ where M is the 2+1 spacetime manifold and the S^1-dimension an internal dimension for the gauge field living in θ.

Using arguments from symmetry-protected topological phases [45–47], which are omitted here but found in Ref. [23], the 't Hooft anomaly for an EFT can be written using a topological action. Stating the final result: the correct anomaly is constructed from a U(1) Chern-Simons action on $M_+ \times S^1$, where M is the boundary of M_+,

$$S = \frac{m}{24\pi^2} \int_{M_+ \times S^1} \epsilon^{ABCDE} A_A \partial_B A_C \partial_D A_E, \tag{3.10}$$

where m admits integer values[6]. Uppercase Latin letters indicate that the internal S^1 direction is included beyond the directions of M_+. The current, $j^A = \frac{\delta S}{\delta A_A}$ incident onto the boundary $M \times S$ then gives the anomalous continuity equation,

$$\partial_A j^A = \frac{m}{8\pi^2} \epsilon^{ABCD} \partial_A A_B \partial_C A_D. \tag{3.11}$$

Note that the indices only range over $M \times S$ now, as indicated by the four indices in the antisymmetric symbol ϵ. The left side of this equation captures the conserved current, and the right side captures the non-conservation when coupled to a gauge field. Conservation of charge on the Fermi surface at each point implies the current along it has to be identically zero. Therefore, what differentiates the U(1) on $M \times S^1$ and LU(1) on M is the left-hand side of the continuity equation, where LU(1) has the additional restriction $j^\theta = 0$. In actuality, there exists scattering between different points on the Fermi surface, breaking LU(1). These are, however, irrelevant perturbations that vanish in the deep IR. Since we are formulating a theory on the IR fixed point [23], we assume $j^\theta = 0$ to hold without any reservations.

Defining a field strength tensor as $F_{AB} = \partial_A A_B - \partial_B A_A$ gives the background electric field $E_i = F_{ti}$ and the magnetic field $2B = \epsilon^{ij} F_{ij}$, where i and j range over the spatial components. By contracting over θ and t, the anomaly equation can be written as

$$\partial_A j^A = \frac{m}{8\pi^2} \left(2\epsilon^{ij} E_i F_{\theta j} + \frac{1}{2} B F_{\theta t} \right). \tag{3.12}$$

[6]The reason for the quantisation of m is to ensure that the total charge of the U(1) subgroup of LU(1) remains an integer. See Ref. [23] for more information

Once more, we make inferences using Fermi liquid theory. When $B = 0$, meaning only a background electric field is coupled to the electrons, we find that the anomaly becomes

$$\partial_A j^A = \frac{m}{(2\pi)^2}\epsilon^{ij}E_i F_{\theta j}. \tag{3.13}$$

The non-conservation of the charge in Fermi liquid theory can be computed exactly to be

$$\partial_A j^A = \frac{1}{(2\pi)^2}\epsilon^{ij}E_i \partial_\theta k_j(\theta), \tag{3.14}$$

where $k_i(\theta)$ is the Fermi surface in momentum space. When comparing (3.13) with (3.14), we identify that $F_{\theta i} = \partial_\theta k_i(\theta)$ for the Fermi liquid [48]. The system is translation invariant, allowing for a gauge-fixing condition $\partial_i A_\theta = 0$ and $\partial_t A_\theta = 0$[7]. In this gauge $\partial_\theta \left[A_i - k_i(\theta)\right] = 0$, where we can identify A_i as the Fermi surface up to an additive constant in θ. We will take for granted that this holds in general when leaving the Fermi liquid, or rather, this identity can be considered the defining relation for the Fermi surface in any ersatz Fermi liquid by construction [21].

What is clear is that a two-dimensional metal has the three characteristics that we used to show Luttinger's theorem for the Luttinger liquid. Once more, we omit the details found in Ref. [23] and state the final result of the generalised Luttinger's theorem.

Generalised Luttinger's theorem.

For any QFT with a $\mathbb{R}^d \times \mathrm{U}(1)$ symmetry where the following is known:

1. The emergent symmetry G_{IR}.
2. The homomorphic mapping to the IR, $\varphi : \mathbb{R}^d \times \mathrm{U}(1) \to G_{\mathrm{IR}}$.
3. The 't Hooft anomaly of the IR theory.

The microscopic charge density ρ can be found in the IR theory.

...

For the two-dimensional ersatz Fermi liquid, the relation is

$$\rho = \frac{m\mathcal{V}_{\mathrm{F}}}{(2\pi)^2}, \tag{3.15}$$

where $\mathcal{V}_{\mathrm{F}}$ is the volume enclosed by the Fermi surface.

Of note is that, once more, there is no mention of what the coupling of the theory is. Thus, by how we defined metals, they will be EFLs that satisfy Luttinger's theorem, regardless of whether they flow to a Fermi liquid or non-Fermi liquid under RG. We conclude that for any holographic model of a non-Fermi liquid, Luttinger's theorem ought to hold.

[7] This latter gauge choice will allow us to write a simple expression for the boundary currents later in (3.21).

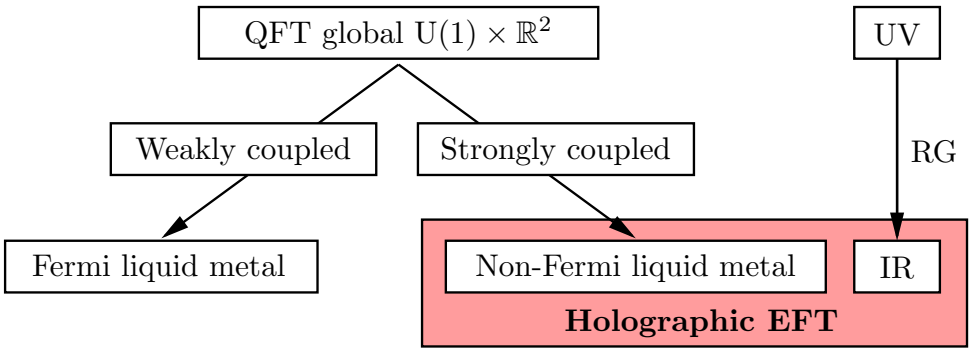

Figure 3.4: The landscape in which ersatz Fermi liquids exist. A holographic effective field theory will describe physics marked by the red square. This is where the relevant operators under RG are those beyond Fermi liquid theory.

3.2 Holographic metals

The standard holographic approach to modelling compressible matter uses a Reissner–Nordström (RN) bulk theory [17]. By the holographic dictionary, we know that the dynamical U(1) gauge field is dual to a global U(1) in the boundary theory, where a non-zero chemical potential generates a charge density. A sample calculation for the RN-bulk can be found in appendix A. Unfortunately, these models do not manage to capture a Fermi surface where Luttinger's theorem holds.

As was discussed in section 2.3.2, a property of holographic models is that they describe the entire RG flow from some unknown QFT Hamiltonian in the UV to the effective IR theory through the geometry of the radial dimension. This is contrary to what one usually does for metals in condensed matter theory, where the UV is of little concern due to the complex Hamiltonians that generally arise. Instead, one only concerns themselves with the IR effective theory emergent at large scales. Indeed, Fermi liquid theory itself can be viewed as an IR fixed point [49].

In Ref. [21], this effective field theory approach is applied to holography. Leaving the idea of describing the entire RG flow from the UV to the IR, a holographic model for the emergent theory is considered instead. The landscape of this discussion can be seen in figure 3.4. The effective field theory of Ref. [21] is the effective field theory of a non-Fermi liquid.

We established what properties the dual boundary theory should have when discussing Luttinger's theorem. What is left is deploying the holographic dictionary of chapter 2 to incorporate these properties in the gravity theory. The boundary theory has a global LU(1) symmetry, which is dual to a dynamic LU(1) gauge field in the bulk. Furthermore, the LU(1) symmetry should have an 't Hooft anomaly. As seen in (3.10), introducing a Chern-Simons term in the action captures the 't Hooft anomaly on the boundary. Furthermore, a gauge field should have a Maxwell term. We need to take care when considering S^1, the Fermi surface dimension, which is not part of the $D = 4$ spacetime manifold M. The θ-dimension should be treated as the "flavour"

index ranging the dimensionality of the gauge group, be it an infinite dimensional index in the case of LU(1). Lastly, the restriction $j^\theta = \frac{\delta S}{\delta A_\theta} = 0$ tells us that the Maxwell action for the gauge field contains no A_θ. The action for the dynamical LU(1) gauge field is then

$$\begin{aligned} S_{\mathrm{M}} + S_{\mathrm{CS}} = &-\frac{1}{4}\int_M \mathrm{d}^4x\sqrt{-g}\int_{S^1}\mathrm{d}\theta\frac{1}{\alpha(\theta)}F_{\mu\nu}(\theta)F^{\mu\nu}(\theta) \\ &+\frac{m}{24\pi^2}\int_{M\times S^1}\mathrm{d}^4x\mathrm{d}\theta\,\epsilon^{ABCDE}A_A\partial_B A_C\partial_D A_E. \end{aligned} \tag{3.16}$$

In the most general case, the coupling constant can depend on θ. The action contains the determinant of the metric, $\sqrt{-g}$, which is governed by the Einstein-Hilbert action. The complete action for the theory is then written as

$$S_{\mathrm{M}} + S_{\mathrm{CS}} + S_{\mathrm{EH}} = S_{\mathrm{M}} + S_{\mathrm{CS}} + \frac{1}{2\kappa^2}\int_M \mathrm{d}^4x\sqrt{-g}\,(2R-\Lambda)\,. \tag{3.17}$$

With the action determined, what remains is to find a background for A_μ around which the linear response of a perturbation can be found. Normally, the boundary theory has a chemical potential that is encoded in a non-trivial A_t in the bulk, giving a microscopic charge density that flows to the IR where it is zero. Here, however, we are not trying to describe the whole IR flow, but rather the IR fixed point of an effective field theory. Therefore, we can conclude that the background should be at zero charge as we only have a Fermi surface. In total, the background is not zero as the defining relation for the Fermi surface found from (3.13) and (3.14) sets the background to $A_i(\theta) = k_i(\theta)$.

With the background established, the necessary prescription for the bottom-up gravity theory is reached. What is left is to use the holographic machinery to extract interesting physics for the effective field theory in the boundary.

3.2.1 Boundary currents

In chapter 2, we showed how to extract results in the boundary using the bulk. In the case of a bulk gauge field, the dual boundary operator was a conserved current. When considering the boundary, the metric is the vacuum AdS metric (2.8) in four dimensions

$$\mathrm{d}s^2 = \frac{L^2}{r^2}\left(-\mathrm{d}t^2+\mathrm{d}x^2+\mathrm{d}y^2+\mathrm{d}r^2\right). \tag{3.18}$$

Unlike the scalar field, we do not need any counter-terms, as there are no divergences at the boundary. To see this, we vary the action with respect to A_μ giving the equations of motion

$$\partial_\nu[\sqrt{-g}F^{\nu\mu}] = \frac{m\alpha(\theta)}{(2\pi)^2}\epsilon^{\mu\nu\rho\sigma}\partial_\theta A_\nu\partial_\rho A_\sigma. \tag{3.19}$$

The left-hand side is the usual covariant Maxwell's equation given by S_{M}. The contribution from S_{CS} is the right-hand side. With the metric (3.18) at the boundary,

it is clear that the left-hand side will determine the order for the leading and subleading terms of the gauge field. We see this as the Chern-Simons term gives one radial derivative at most. The boundary behaviour will, therefore, be the same as a free U(1) gauge field appendix A with $d = 2$,

$$A_\mu(r) = A_\mu^{(0)} + A_\mu^{(1)} r + \text{h.o.t.} \tag{3.20}$$

Another issue is the Chern-Simons contribution to the current terms $\frac{\delta S}{\delta A_\mu}$ in the presence of a boundary. An argument can be made for how to sidestep this issue by considering two copies of the theory with the same background, connected at the boundary. This gives a closed manifold, and the ambiguities surrounding the Chern-Simons term vanish. We refer the reader to Ref. [21] for a full motivation, and instead claim that the current should be the same as for a U(1) gauge field with a total minus sign

$$j^\mu = -\frac{\sqrt{-g}}{\alpha(\theta)} F^{r\mu}\Big|_{r=0}. \tag{3.21}$$

Note that the equations of motion with this current obey the anomalous continuity equation (3.11) summed over θ with the gauge fixing condition that identifies A_i with the Fermi surface.

3.2.2 Correlation functions at zero temperature

The simplest possible case to solve the effective theory for the non-Fermi liquid is for zero temperature and a circular Fermi surface. While this does allow for analytical solutions we make use of Mathematica [50] for some intermediate symbolic manipulation. Since the equations of motion contain no ∂_θ we can solve for each θ separately. We will therefore evaluate at $\theta = 0$ and generalise to all θ by a coordinate argument using the symmetry of the circle.

When considering zero temperature, the metric takes the form of (3.18) throughout the bulk. Furthermore, the equations of motion (3.19) can be linearised by considering the perturbations $a_\mu(x)$ about the background $A_i = k_i(\theta)$. Much like in the case of the scalar field, a plane wave ansatz is made, and with our given gauge freedom, the radial gauge is chosen $A_r = 0$. In totality this means the gauge field, when linearising, has the form $A_i = k_i(\theta) + a_i(r,\theta)\mathrm{e}^{-i\omega t + i(q_x x + q_y y)}$, where $i = x, y$, and $A_t = a_t(r,\theta)\mathrm{e}^{-i\omega t + i(q_x x + q_y y)}$. Note that we have yet to use the freedom to choose the directionality of x and y. We write out the equations in (3.19), meaning $\mu = t, x, y$, and find that

$$\partial_r^2 a_t + \frac{\alpha m}{(2\pi)^2}\left(\partial_\theta k_x \partial_r a_y - \partial_\theta k_y \partial_r a_x\right) - \left(q_x^2 + q_y^2\right) a_t - \omega q_x a_x - \omega q_y a_y = 0 \tag{3.22a}$$

$$\partial_r^2 a_x - \frac{\alpha m}{(2\pi)^2}\partial_\theta k_y \partial_r a_t + \omega q_x a_t + \left(\omega^2 - q_y^2\right) a_x + q_x q_y a_y = 0 \tag{3.22b}$$

$$\partial_r^2 a_y + \frac{\alpha m}{(2\pi)^2}\partial_\theta k_x \partial_r a_t + \omega q_y a_t + q_x q_y a_x + \left(\omega^2 - q_x^2\right) a_y = 0. \tag{3.22c}$$

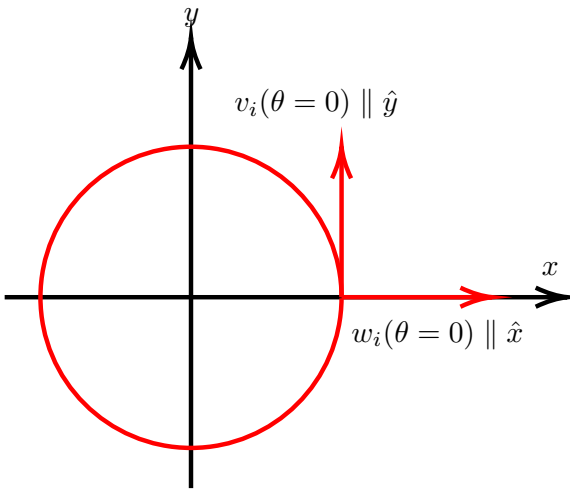

Figure 3.5: The generality of the solution at $\theta = 0$ for a circular Fermi surface in x and y mapped onto perpendicular ($\perp$) and tangential ($\parallel$) coordinates given by the vectors w_i and v_i. The Cartesian unit vectors are the hatted $\hat{x}$ and $\hat{y}$.

This can be rewritten as a matrix equation $\partial_r^2 \mathbf{a} + \Omega \partial_r \mathbf{a} + \Gamma \mathbf{a} = 0$,

$$\partial_r^2 \mathbf{a} + \begin{bmatrix} 0 & -u_y & u_x \\ -u_y & 0 & 0 \\ u_x & 0 & 0 \end{bmatrix} \partial_r \mathbf{a} + \begin{bmatrix} -(q_x^2 + q_y^2) & -\omega q_y & -\omega q_x \\ \omega q_x & \omega^2 - q_y^2 & q_x q_y \\ \omega q_y & q_x q_y & \omega^2 - q_y^2 \end{bmatrix} \mathbf{a} = 0 \tag{3.23}$$

where $\mathbf{a} = (a_t, a_x, a_y)^T$ and $u_i = \alpha m \partial_\theta k_i / 4\pi^2$. Here, the bold letters indicate three component vectors. We now orient our spatial coordinates such that $u_x = 0$, leaving only $-u_y \equiv -u$ in Ω. The meaning of this coordinate choice is made clear in figure 3.5. Due to the symmetry of the circle, we can identify x as a coordinate perpendicular ($\perp$) to the Fermi surface and y as tangential ($\parallel$). The $\theta = 0$ solution can be generalised to any θ in this coordinate system. Introducing the vectors $w_i(\theta) = k_i / k_\mathrm{F}$ and $v_i = \partial_\theta k_i / k_\mathrm{F}$, where the spatial index is raised and lowered by δ^{ij}, we can project q_i as

$$q_\perp = w^i q_i, \qquad q_\parallel = v^i q_i. \tag{3.24}$$

The same projection can be performed to go between spatial x and y dimensions and the perpendicular and tangential frame for any other vector.

The differential equation is solved by $\mathbf{a}_\lambda e^{\lambda r}$, which we can substitute into (3.23), giving $\lambda^2 \mathbf{a}_\lambda + \Omega \lambda \mathbf{a}_\lambda + \Gamma \mathbf{a}_\lambda = 0$, to which solutions exist if $\det(\lambda^2 \mathbb{1}_3 + \lambda \Omega + \Gamma) = 0$. Solving for λ, we find 6 solutions. There is a double root at zero and another four solutions as

$$\begin{aligned} \lambda_\pm &= -\sqrt{q_\perp^2 + q_\parallel^2 - \omega^2 + \frac{1}{2}\left(u^2 \pm \sqrt{u^4 + 4u^2 q_\parallel^2}\right)} \\ \lambda'_\pm &= \sqrt{q_\perp^2 + q_\parallel^2 - \omega^2 + \frac{1}{2}\left(u^2 \pm \sqrt{u^4 + 4u^2 q_\parallel^2}\right)}. \end{aligned} \tag{3.25}$$

The general solution then becomes

$$\mathbf{a} = c_0\mathbf{a}_0 + c_1\left(\mathbf{a}_0 r + \mathbf{a}_1\right) + c_2\mathbf{a}_+ \mathrm{e}^{\lambda_+ r} + c_3\mathbf{a}_- \mathrm{e}^{\lambda_- r} + c_4\mathbf{a}'_+ \mathrm{e}^{\lambda'_+ r} + c_5\mathbf{a}'_- \mathrm{e}^{\lambda'_- r}. \tag{3.26}$$

We see that c_1, c_4 and c_5 must be zero, as we require the solutions to be regular in the bulk. This leaves three $\mathbf{a}_\lambda$, which must be solved for. Starting with $\Gamma\mathbf{a}_0 = 0$, this is solved with $\mathbf{a}_0 = (-\omega, q_\perp, q_\parallel)^\intercal$. The remaining $\mathbf{a}_\pm$ give rather unpleasant expressions. We can circumvent this by looking at the $|\omega|, |\mathbf{q}| \ll u$ regime, which allows us to write $\lambda_+ = -u$, $\lambda_- = -\sqrt{q_\perp^2 - \omega^2}$ in the large k_F limit. This limit will be motivated later. It is considered valid for now, since we are considering an effective field theory. The resulting $\mathbf{a}$:s are

$$\mathbf{a}_+ = \begin{bmatrix} 1 \\ -1 \\ 0 \end{bmatrix}, \quad \mathbf{a}_- = \begin{bmatrix} 0 \\ 0 \\ 1 \end{bmatrix} \tag{3.27}$$

allowing us to finally write the solutions to the perturbations as

$$\mathbf{a} = c_0\mathbf{a}_0 + c_2\mathbf{a}_+ \mathrm{e}^{-ur} + c_3\mathbf{a}_- \mathrm{e}^{-\sqrt{q_\perp^2 - \omega^2}r}. \tag{3.28}$$

The constants, c_0, c_2, and c_3, are determined by the "$\phi \to h$" boundary condition,

$$\begin{aligned} &\mathcal{A}_t = -\omega c_0 + c_2, \quad \mathcal{A}_\perp = q_\perp c_0 - c_2, \quad \mathcal{A}_\parallel = q_\parallel c_0 + c_3 \implies \\ &c_0 = \frac{\mathcal{A}_t + \mathcal{A}_\perp}{q_\perp - \omega}, \quad c_2 = \frac{q_\perp \mathcal{A}_t + \omega \mathcal{A}_\perp}{q_\perp - \omega}, \quad c_3 = \mathcal{A}_\parallel + \frac{(\mathcal{A}_t + \mathcal{A}_\perp)\, q_\parallel}{\omega - q_\perp}, \end{aligned} \tag{3.29}$$

where $\mathcal{A}_\mu$ denotes the dual gauge field on the boundary.

Having solved the equations of motion, (3.21) can be used to evaluate the currents. As u is taken to be large compared to all other scales in the effective theory, the solution can be truncated to the two leading terms in a series expansion in u^{-1}. When written in terms of the perturbing electric field, $E_\perp = -\mathrm{i}(\omega\mathcal{A}_\perp + q_\perp\mathcal{A}_t)$, $E_\parallel = -\mathrm{i}(\omega\mathcal{A}_\parallel + q_\parallel\mathcal{A}_t)$, and the magnetic field $B = \mathrm{i}(q_\perp\mathcal{A}_\parallel - q_\parallel\mathcal{A}_\perp)$, the currents are found to be

$$\langle j^t \rangle = -\langle j^\perp \rangle = -\mathrm{i}\frac{m|\partial_\theta \mathbf{k}|}{(2\pi)^2}\frac{E_\perp}{\omega - q_\perp} + \mathrm{i}\alpha^{-1}\frac{(\omega + q_\perp)q_\parallel}{(\omega - q_\perp)\sqrt{-\omega^2 + q_\perp^2}}(E_\parallel + B) + \mathcal{O}\left(k_\mathrm{F}^{-1}\right) \tag{3.30a}$$

$$\langle j^\parallel \rangle = -\mathrm{i}\alpha^{-1}\frac{(\omega + q_\perp)}{\sqrt{-\omega^2 + q_\perp^2}}(E_\parallel + B) + \mathcal{O}\left(k_\mathrm{F}^{-1}\right). \tag{3.30b}$$

In the language of the renormalisation group, the $\mathcal{O}(k_\mathrm{F}^{-1})$-terms describe the influence of irrelevant operators with k_F constituting a cutoff. This is seen by the fact that ω/k_F and $|\mathbf{q}|/k_\mathrm{F}$ go to zero for large k_F. Technically, we are not describing a fixed point when dropping the higher-order terms, but rather a one-parameter trajectory as the irrelevant k_F^0-order terms remain.

By taking a functional derivative with respect to $\mathcal{A}_t$ of (3.30a), we arrive at the density-density correlator,

$$\langle j^t(\theta)j^t(\theta')\rangle = \frac{\delta\langle j^t(\theta)\rangle}{\delta\mathcal{A}_t(\theta')} = \left(-\frac{m|\partial_\theta \mathbf{k}|}{(2\pi)^2}\frac{q_\perp}{\omega - q_\perp} + \frac{(\omega+q_\perp)q_\parallel^2}{(\omega-q_\perp)\sqrt{-\omega^2+q_\perp^2}}\right)\delta(\theta-\theta'). \tag{3.31}$$

The real pole at $\omega = q_\perp$ signifies a propagating mode. In our units, the mode propagates at light speed in the bulk. As it turns out, the speed of light in the bulk corresponds to the Fermi velocity on the boundary [17]. Therefore, the pole at $\omega = q_\perp$ signifies that the mode moves perpendicular to the Fermi surface at the Fermi velocity. This is the same result as one finds in Fermi liquid theory with the Landau interactions set to zero. One should not interpret this as our theory being weakly coupled like Fermi liquid theory. Rather, it should be seen as a general outcome when considering the hydrodynamics of theories with a Fermi surface [21, 51]. The fact that we do not have a Fermi liquid is reflected in the second term, which is not present for Fermi liquids. The presence of the branch cut, $\sqrt{-\omega^2+q_\perp^2}$, is indicative of the lack of quasiparticles [17], implying that we are in non-Fermi liquid territory.

Taking limits of two-point functions gives interesting properties of the metal. One such property is the static charge susceptibility

$$\chi(\theta,\theta') = \lim_{q\to 0}\lim_{\omega\to 0}\frac{\partial\langle j^t(\theta)\rangle}{\partial A_t(\theta')} = \frac{m|\partial_\theta \mathbf{k}(\theta)|}{(2\pi^2)}\delta(\theta-\theta'). \tag{3.32}$$

The total charge susceptibility we find by integrating the contributions from the whole Fermi surface,

$$\chi = \int \mathrm{d}\theta\mathrm{d}\theta'\frac{m|\partial_\theta \mathbf{k}(\theta)|}{(2\pi^2)}\delta(\theta-\theta') = \frac{m}{(2\pi)^2}\int \mathrm{d}\theta|\partial_\theta \mathbf{k}(\theta)| = \frac{m}{(2\pi)^2}l_F \tag{3.33}$$

where l_F is the length of the Fermi surface.

Next, we want to evaluate the optical conductivity. This is done by letting $\mathbf{q}\to 0$ and setting $B = 0$. Thus, we look at the current produced from an external perturbing electric field. From (3.30a) and (3.30b) we find the currents,

$$\langle j^\perp\rangle = \mathrm{i}\frac{m|\partial_\theta \mathbf{k}(\theta)|}{(2\pi)^2}\frac{E_\perp}{\omega}, \qquad \langle j^\parallel\rangle = \alpha^{-1}(\theta)E_\parallel. \tag{3.34}$$

Here we have chosen the branch for the square root as $\sqrt{-\omega^2+q_\perp^2} = -\mathrm{i}\sqrt{\omega^2-q_\perp^2}$ when $|\omega| > |q_\perp|$. In general, the conductivity is given as a tensor of the form

$$j^i(\omega) = \sigma^{ij}(\omega)E_j(\omega). \tag{3.35}$$

Again, we must consider the contribution from the whole Fermi surface by integrating over θ. The solution consists of a reactive *"Drude conductivity"* at infinite scattering time, which is the contribution from the leading term of the current perpendicular

to the Fermi surface, $\langle j^{\perp}\rangle$. The current tangential to the Fermi surface, $\langle j^{\parallel}\rangle$, gives a frequency independent *"incoherent conductivity"*,

$$\sigma(\omega) = \mathcal{D}\frac{\mathrm{i}}{\omega} + \sigma_{\mathrm{inc}} + \mathcal{O}\left(k_{\mathrm{F}}^{-1}\right), \tag{3.36}$$

where

$$\mathcal{D}^{ij} = \frac{m}{(2\pi)^2}\int \mathrm{d}\theta\, w^i(\theta)w^j(\theta)|\partial_\theta \mathbf{k}(\theta)|, \qquad \sigma_{\mathrm{inc}}^{ij} = \int \mathrm{d}\theta\, v^i(\theta)v^j(\theta)\alpha(\theta)^{-1}. \tag{3.37}$$

Since the LU(1) symmetry assumes translational invariance, and therefore also momentum conservation, the infinite Drude peak at $\omega = 0$ seen in the dissipative term in the conductivity is expected. The same result would be found in Fermi liquid theory. One can think of this as a quality inherent to any system with a Fermi surface and momentum conservation [21]. The dissipative incoherent term, σ_{inc}, arises from the current tangential to the Fermi surface. In Fermi liquid theory, modes only ever travel perpendicular to the Fermi surface at Fermi velocity when Landau interactions are set to zero [21, 51]. Thus, the strongly coupled physics is reflected in the emergence of σ_{inc}.

4. Holographic EFT: finite temperature

Leaving the zero-temperature case, which has been presented in Ref. [21], we now wish to turn on a temperature for the holographic model. The holographic dictionary states that this is done by introducing a black hole with a horizon at r_+ where the temperature is given by (2.49). Unfortunately, the equations of motion are then no longer analytically solvable, regardless of the shape of the Fermi surface. Therefore, the evaluation of responses at non-zero temperatures has to be computed with numerical methods.

The first section of this chapter presents the methods used to solve the equations of motion. The code is based on code by Ref. [52] and is written in Mathematica using xAct packages [53–57] for handling tensorial calculations. The differential equations are solved using pseudospectral methods [58], as is common in holographic numerics [59–61].

Given a method of solving the equations of motion, we examine the temperature behaviour and see how it compares with the zero-temperature case. Further, we examine the behaviour specific to non-Fermi liquids. Much like before, we take limits of two-point functions to evaluate charge susceptibility and optical conductivity, which are now explicitly evaluated but at finite temperatures. There are some subtleties since we are considering an effective theory. As is argued in [21], the effective theory concerns the $k_{\mathrm{F}} \gg T, |\omega|, |\mathbf{q}|$ regime. For numerical calculations this condition will be replaced by an explicit cutoff scale, the value of which we will motivate from physical arguments and the numerical results.

4.1 Scheme for evaluation

When considering the same theory at finite temperature, the action is unchanged. Thus, the equations of motion are found by varying the action with respect to the fields as usual. Varying the metric gives Einstein's equations

$$R_{\mu\nu} - \frac{1}{2} g_{\mu\nu} \left(R + 2\Lambda\right) = F_{\mu\kappa} F^{\kappa}_{\nu} - \frac{1}{4} g_{\mu\nu} F_{\kappa\lambda} F^{\kappa\lambda}, \tag{4.1}$$

where, in four dimensions, we have $\Lambda = 3/L^2$. The stress-energy tensor has the usual form for an RN theory, as the topological Chern-Simons term has no metric. Varying the gauge field gives the same Maxwell's equation as (3.19) seen before.

Turning on a temperature does not affect the background for the gauge field. We are

free to choose any exotic Fermi surface we want. The metric, however, cannot be (3.18) throughout the bulk anymore. As was discussed in section 2.3.3, a boundary QFT at finite temperature translates to a black hole in the bulk and thus an emblackening factor, $f(r)$, in the metric. Furthermore, we found a regularity requirement for the fields in the deep interior $r \to \infty$ for both the scalar and LU(1) fields. The corresponding requirement when the bulk has a horizon at r_+, is the so-called *infalling boundary conditions*. Infalling boundary conditions impose a requirement for modes to temporally carry energy into the black hole, rather than out of it. The simplest way to do this is to change coordinates to infalling Eddington-Finkelstein coordinates, where the time coordinate is transformed as $\mathrm{d}t = \mathrm{d}u + \mathrm{d}r/f(r)$. The background for the metric (2.43) in four dimensions and the gauge field then becomes

$$\begin{aligned} \mathrm{d}s^2 &= \frac{L^2}{r^2}\left(-f(r)\mathrm{d}u^2 - 2\mathrm{d}u\mathrm{d}r + \mathrm{d}x + \mathrm{d}y\right), \\ A_i &= k_i(\theta), \quad A_u = A_r = 0, \end{aligned} \tag{4.2}$$

where $f(r)$ is the emblackening factor. The vector $k_i(\theta)$ is the parametrisation of the Fermi surface with $i = x, y$. Infalling Eddington-Finkelstein coordinates together with the relation between the generating current and bulk fields, "$\phi \to h$" found in section 2.3, completely fixes the Dirichlet problem from the boundary to the horizon.

Substituting the background ansatz into Einstein's equations gives an equation for the emblackening factor. The field strength tensor is zero since the gauge field background is independent of the manifold directions, u, x, y and r. This means that the stress-energy tensor in (4.1) must be zero for the background. Solving for $f(r)$ with the usual boundary conditions, $f(r_+) = 0$, gives

$$3 - 3f(r) + rf'(r) = 0 \implies f(r) = 1 - \frac{r^3}{r_+^3}. \tag{4.3}$$

From (2.49) the horizon gives the temperature as $T = 3/(4\pi r_+)$.

We have reached the starting point for evaluating linear responses. Considering perturbations about the background for the metric and gauge field we have $g_{\mu\nu} \to g_{\mu\nu} + \delta g_{\mu\nu}$ and $A_\mu \to A_\mu + \delta A_\mu$, which gives the linearised equations of motion for the perturbations. Ten of these are Einstein's equations and four are Maxwell's equations,

$$\begin{aligned} \delta G_{\mu\nu} + \delta g_{\mu\nu}\Lambda &= \delta T_{\mu\nu} \\ \nabla_\mu \delta F^{\mu\nu} &= \delta J^\nu. \end{aligned} \tag{4.4}$$

The δ in front of each tensor indicates that it has been linearised in the perturbations, where $G_{\mu\nu}$ is the Einstein tensor, $T_{\mu\nu}$ the energy-stress tensor, and J^ν the Chern-Simons contribution to (3.19).

The system has a gauge redundancy as we have yet to choose any gauge. One option would be to choose the radial gauge as before, setting all radial components to zero. With this, we would have to account for pure gauge modes [62, 63]. Instead, we

will use what is referred to as the *"DeTurck trick"* [64], which deals with the gauge redundancy in a manner akin to a Lagrange multiplier. By adding the terms

$$\begin{aligned} \tau_\mu &= \nabla^\kappa \left(\delta g_{\kappa\mu} - \frac{1}{2} g_{\kappa\mu} \delta g^\lambda_\lambda \right) \\ \chi &= \nabla^\kappa \delta A_\kappa \end{aligned} \tag{4.5}$$

to the equations of motion as

$$\begin{aligned} &\delta G_{\mu\nu} + \delta g_{\mu\nu} \Lambda - \nabla_{(\mu} \tau_{\nu)} = \delta T_{\mu\nu} \\ &\nabla_\mu \delta F^{\mu\nu} + \nabla^\nu \chi = \delta J^\nu, \end{aligned} \tag{4.6}$$

all gauge redundancy is fixed. All that remains is solving the coupled equations.

Before discussing how to solve the equations, we look at their form. The stress-energy tensor $\delta T_{\mu\nu}$ is quadratic in F, which contains no gauge background due to the spatiotemporal derivatives. It therefore has to be quadratic in the perturbations δA, which is zero to linear order. Similarly, the left-hand side of Maxwell's equation is linear in perturbations, meaning only the background of the metric can contribute. The Chern-Simons term contains θ derivatives but has no metric contribution at all. We can conclude that the perturbations for the metric and gauge fields are completely decoupled and can be solved separately. As the novel results lay in the gauge field, we will disregard the metric fluctuations from here on out. We will discuss the meaning of this in the next chapter.

Once more, we make a plane wave ansatz for the perturbations $\delta A_\mu(r) \mathrm{e}^{-\mathrm{i}\omega + \mathrm{i}x q_x + \mathrm{i}y q_y}$. The result is four ordinary differential equations in r. A suitable technique for solving these types of Dirichlet boundary problems, which generally arise in holographic numerics, is the *"pseudospectral algorithm"* [58–61]. We employ it in the exact formulation as given in [52].

Pseudospectral algorithm

Imagine a set of n_f bulk fields, $\Phi_i(z)$, where z ranges from the boundary at $z = 0$ to the horizon at $z = 1$, and an equal number of second-order coupled linear differential equations with given boundary conditions

$$\begin{aligned} \hat{\mathcal{L}}\phi = \left[\alpha_{ij}(z) \partial_z^2 + \beta_{ij}(z) \partial_z + \gamma_{ij}(z) \right] \Phi_i = 0 \\ \text{b.c.} \begin{cases} \Phi_i(z=0) = \dots \\ \Phi_i(z=1) = \dots . \end{cases} \end{aligned} \tag{4.7}$$

In our case, Φ_i only contains the $n_f = 4$ fields of the gauge field perturbations, $\Phi_i = \{\delta A_u, \delta A_x, \delta A_y, \delta A_z\}^a$. The pseudospectral algorithm solves the differential equations at discrete values of $z = z_l$ with $l = 1, \dots N$, where the z_l are placed on a so-called Chebyshev-Lobatto grid [58]. For our intents and

purposes, the grid is modified somewhat to be

$$z_l = \frac{1}{2}\left(1 - \cos\left[\pi \frac{l-1}{N-1}\right]\right). \tag{4.8}$$

As is clear from (4.8), the first point is $z_1 = 0$ and the final point $z_N = 1$. With explicit points given, the differential operator can be written using a dense matrix, D_{mn}. Thus, (4.7) becomes

$$L_{pq}\phi_q = \left(D^2_{mn} \otimes \alpha_{ij} + D_{mn} \otimes \beta_{ij} + \delta_{mn} \otimes \gamma_{ij}\right)\phi_q = 0 \tag{4.9}$$

where $\otimes$ denotes a Kronecker product. The first n_f rows of ϕ_q correspond to $\Phi_i(z_1)$, the next n_f rows with $\Phi_i(z_2)$, and so on up to $\Phi_i(z_N)$. Since z_1 is the boundary, we can modify the first n_f rows of L_{pq} to set the boundary values of the fields at $z = 0$. The first n_f rows in the left-hand side are changed to $\delta_{1n} \otimes \delta_{ij}$ together with the right-hand side of (4.9) being set to $F_p = \Phi_p(z = 0)$ for $p = 1, \ldots, n_f$, and $F_p = 0$ for $p = n_f + 1, \ldots, n_f \times N$. The boundary conditions at $z = 1$ are already dealt with by choosing infalling Eddington-Finkelstein coordinates and thus we do not need to change the rows corresponding to $z = 1$. The result is a linear matrix equation

$$L_{pq}\phi_q = F_p. \tag{4.10}$$

Solving this equation gives the values of the fields at each grid point of z

$$\phi_i(z_l) = \phi_{i(l-1)+1}. \tag{4.11}$$

[a] We saw an example of this type of equation in (3.23).

As stated above, the algorithm has r ranging from 0 to 1. To use it, we need to make the coordinate transformation $r = zr_+$. With this coordinate change, the pseudospectral algorithm can be applied to (4.6), which gives an approximate solution to all four equations. Having solved the gravity theory using this algorithm, the dual currents on the boundary can be evaluated using (3.21), keeping in mind the coordinate changes.

In the remainder of this chapter, we compute correlation functions using the aforementioned method. We make calculations for different temperatures, including "$T \to 0$". Due to the nature of this numerical implementation, there is no real way of going to $T = 0$ as this implies a horizon r_+ at ∞. Instead, the horizon will be set to be as far away as the numerics allow while still having converging solutions. In our case, this is $10^4 \cdot T = k_{\mathrm{F}}$. As a reference, we can consider a Fermi energy of 10 eV, with a corresponding lowest temperature of ~ 10 K at the lowest.

4.2 Correlation functions at finite temperature

Before evaluating the responses, we should consider the scale of interest of the theory. For the zero temperature case, we went to the $k_F \gg |\omega|, |\mathbf{q}|$ limit. At finite temperature T, we need another scale $k_F \sim T$. Relevant temperatures when considering metals are around $T \sim 300$ K, which in natural units is ~ 0.025 eV. In contrast, we can expect Fermi energies of the order $k_F \sim 10$ eV. Thus, we will consider energies up to $k_F \sim 400T$.

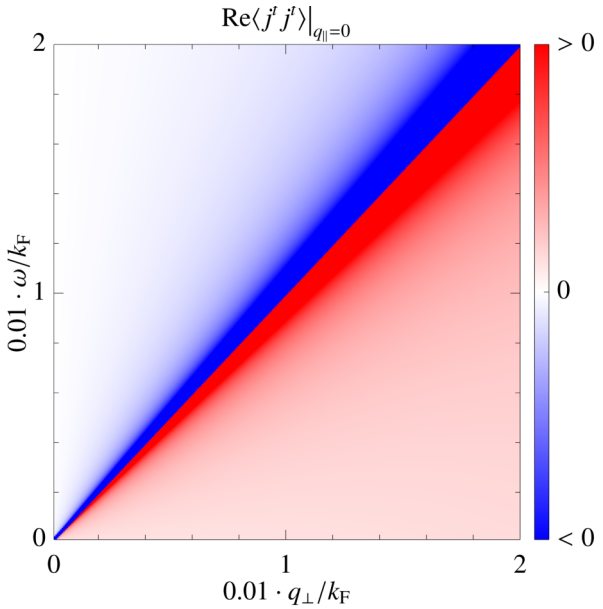

Figure 4.1: The real part of the density two-point function with $q_\parallel = 0$ at $T \to 0$. The discontinuity along $\omega = q_\perp$ shows the perpendicular propagating mode. Red indicates positive values, and blue indicates negative values.

As we now evaluate numerically, we also need an explicit cutoff for ω and $\mathbf{q}$ to examine up to. With $k_B T \sim \hbar\omega$, we expect the same scale for ω and $\mathbf{q}$ as for the temperature to see both thermal effects and effects due to the perturbing field. Therefore, we should set a cutoff above $400\omega \sim k_F$. Consider the ratios for the cutoff in ω and $\mathbf{q}$,

$$\frac{\omega}{k_F} < \omega_\Lambda = 0.02, \qquad \frac{|\mathbf{q}|}{k_F} < q_\Lambda = 0.02. \tag{4.12}$$

We see in figure 4.1 that the expected behaviour holds within $\omega = \omega_\Lambda k_F$ and $q_\perp = q_\Lambda k_F$. This can be considered a numerical justification for dropping the higher order terms in (3.30a) and (3.30b) for the effective theory. We take these ratios to be the UV cutoff scale, meaning we will examine the behaviour of the currents at finite temperature up to this cutoff; more explicit justification for these cutoffs can be found in appendix B. The exact value for the cutoff is arbitrary so long as the irrelevant terms in (3.30a) and (3.30b) do not contribute. One could consider going beyond this cutoff to see when the higher-order terms do contribute, constituting a more explicitly motivated cutoff. For our intents and purposes, however, we will settle with ω_Λ and q_Λ, as we would otherwise be going far past the range we are trying to investigate.

In the zero temperature case, the Fermi surface was set to be a circle at some Fermi momentum k_F, $\mathbf{k} = k_F(\cos[\theta], \sin[\theta])$. This restriction has been lifted for numerical calculations, and we can choose any surface. Nonetheless, the Fermi surface is set to be a circle, allowing for the same identification between x, y and $\perp, \parallel$ at $\theta = 0$. We will also set $\alpha(\theta) = 1$ independent of θ. The solutions scale identically with m

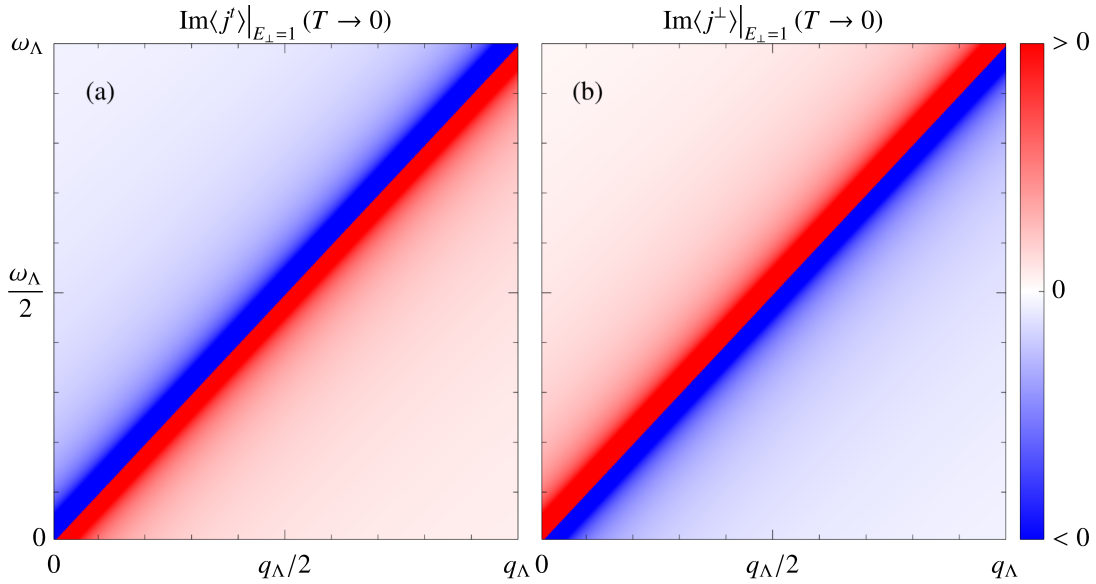

Figure 4.2: The imaginary part of the current response, $\langle j^t \rangle$ can be seen in (a) and likewise for $\langle j^\perp \rangle$ in (b), at $T \to 0$ when perturbed by an electric field perpendicular to the Fermi surface. A clear discontinuity along $\omega = q_\perp$ shows the expected pole. Red indicates positive values, and blue indicates negative values.

and k_F, meaning that we only need to tune the product mk_F to see how the theory responds to changes in either value. Therefore, we set $m = 1$. For more information about the numerics, see appendix B.

Currents at $E_\perp = 1$

We want to evaluate the currents at different temperatures and see how they differ compared to (3.30a) and (3.30b) at finite temperatures. The best way to do this is to see how each term in the expansions changes separately. We can examine the first term of (3.30a) by turning on an electric field perpendicular to the Fermi surface as shown in figure 3.5. Experimentally, such an electric field is impossible, of course; this should be thought of as a theoretical probe to examine the terms for the currents separately. By setting $\mathcal{A}_x = 1$ and $\mathcal{A}_u = \mathcal{A}_y = \mathcal{A}_z = 0$ as boundary conditions at $z = 0$ in (4.10) and evaluating at $\theta = 0$ we find $-\mathrm{i}\omega\langle j^\mu \rangle|_{E_\perp=1}$. In our implementation, the current and boundary gauge field is inherently at the same θ.

Indeed, we have a pole at $\omega = q_\perp$ in $\mathrm{Im}\langle j^t \rangle$ for $T/k_\mathrm{F} \to 0$ as seen in figure 4.2. There is no significant difference between $\langle j^t \rangle$ and $-\langle j^\perp \rangle$ beyond numerical error as expected,

$$\max_{\{q_\Lambda, \omega_\Lambda\}} \left| \frac{\langle j^t \rangle + \langle j^\perp \rangle}{k_\mathrm{F}} \right| \approx 0.25 \ll \max_{\{q_\Lambda, \omega_\Lambda\}} \left| \frac{\langle j^t \rangle}{k_\mathrm{F}} \right| \approx \max_{\{q_\Lambda, \omega_\Lambda\}} \left| \frac{\langle j^\perp \rangle}{k_\mathrm{F}} \right| \approx 4000, \tag{4.13}$$

where $\{q_\Lambda, \omega_\Lambda\}$ is the numerical grid spanning $q_\perp$ and ω. The tangential current $\langle j^\parallel \rangle$ and the real parts of $\langle j^t \rangle$ and $\langle j^\perp \rangle$ are zero everywhere in $\{q_\Lambda, \omega_\Lambda\}$. We can conclude

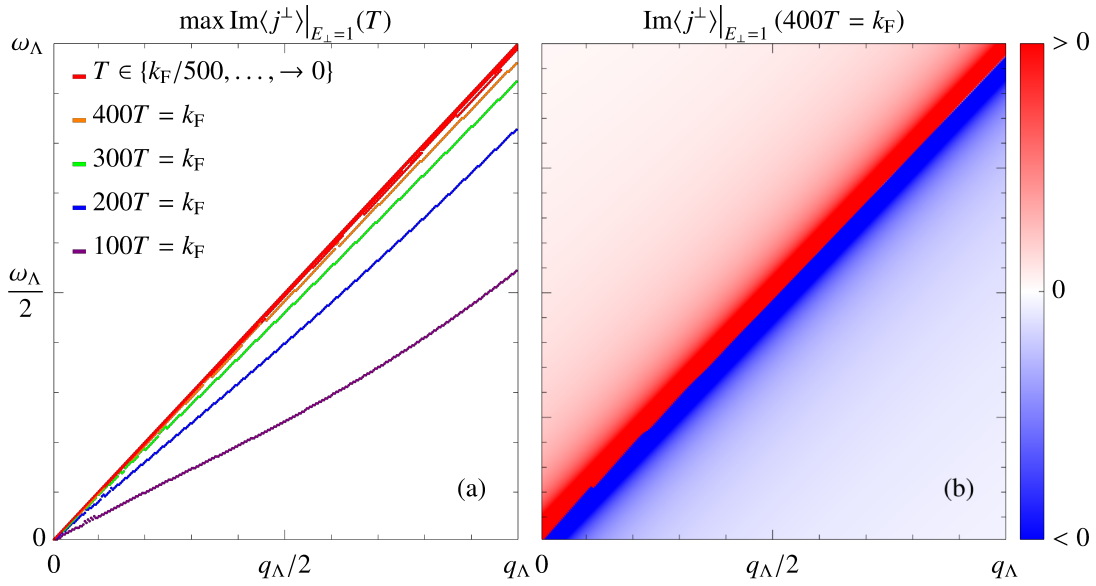

Figure 4.3: (a) shows the maximum of the imaginary part for each $q_\perp$ of the current response at temperatures between $T \to 0$ and $100T = k_\mathrm{F}$ when perturbed by an electric field perpendicular to the Fermi surface. In (b) shows $\langle j^\perp \rangle$ at $400T = k_\mathrm{F}$. A pole runs along $\omega = q_\perp$ similar to $T \to 0$ seen in figure 4.2. Red indicates positive values, and blue indicates negative values.

that the currents behave precisely as predicted by the analytical evaluation at $T \to 0$ within q_Λ and ω_Λ. With this unsurprising result as a control, we now increase the temperature.

As the temperature increases, the dispersion relation shifts down slightly, as seen in figure 4.3 (a). The change is seen most clearly when going past $400T = k_\mathrm{F}$ to the temperatures $300T \geq k_\mathrm{F}$. When remaining at temperatures considered relevant for metals, the pole for $\langle j^\perp \rangle$ (and $\langle j^t \rangle$) is essentially unaffected. The current at $400T = k_\mathrm{F}$ can be seen in figure 4.3 (b). In comparison to the current at zero temperature seen in figure 4.2, there is little difference. The tangential current, $\langle j^\parallel \rangle$, is still zero regardless of temperature. We can conclude that all the behaviours in the zero temperature analysis remain for finite temperatures at scales of interest for the leading term of (3.30a).

Currents at $E_\parallel = 1$

To examine the behaviour of the subleading terms in (3.30a) and (3.30b), we instead want to turn on an electric field tangential to the Fermi surface. By setting $\mathcal{A}_y = 1$ and $\mathcal{A}_u = \mathcal{A}_x = \mathcal{A}_z = 0$ as boundary conditions at $z = 0$ in (4.10) and evaluating at $\theta = 0$ we now are considering $-\mathrm{i}\omega \langle j^\mu \rangle_{E_\parallel = 1}$.

First, consider the subleading term in $\langle j^\mu \rangle$, for $\mu = t, \perp$ at $T \to 0$. To get a contribution to the currents, we need $q_\parallel \neq 0$. We set $q_\parallel = q_\Lambda k_\mathrm{F}/10$ to stay near relevant scales. For $\langle j^\perp \rangle$, the expected branch cut and mode at $\omega = q_\perp$ can be seen

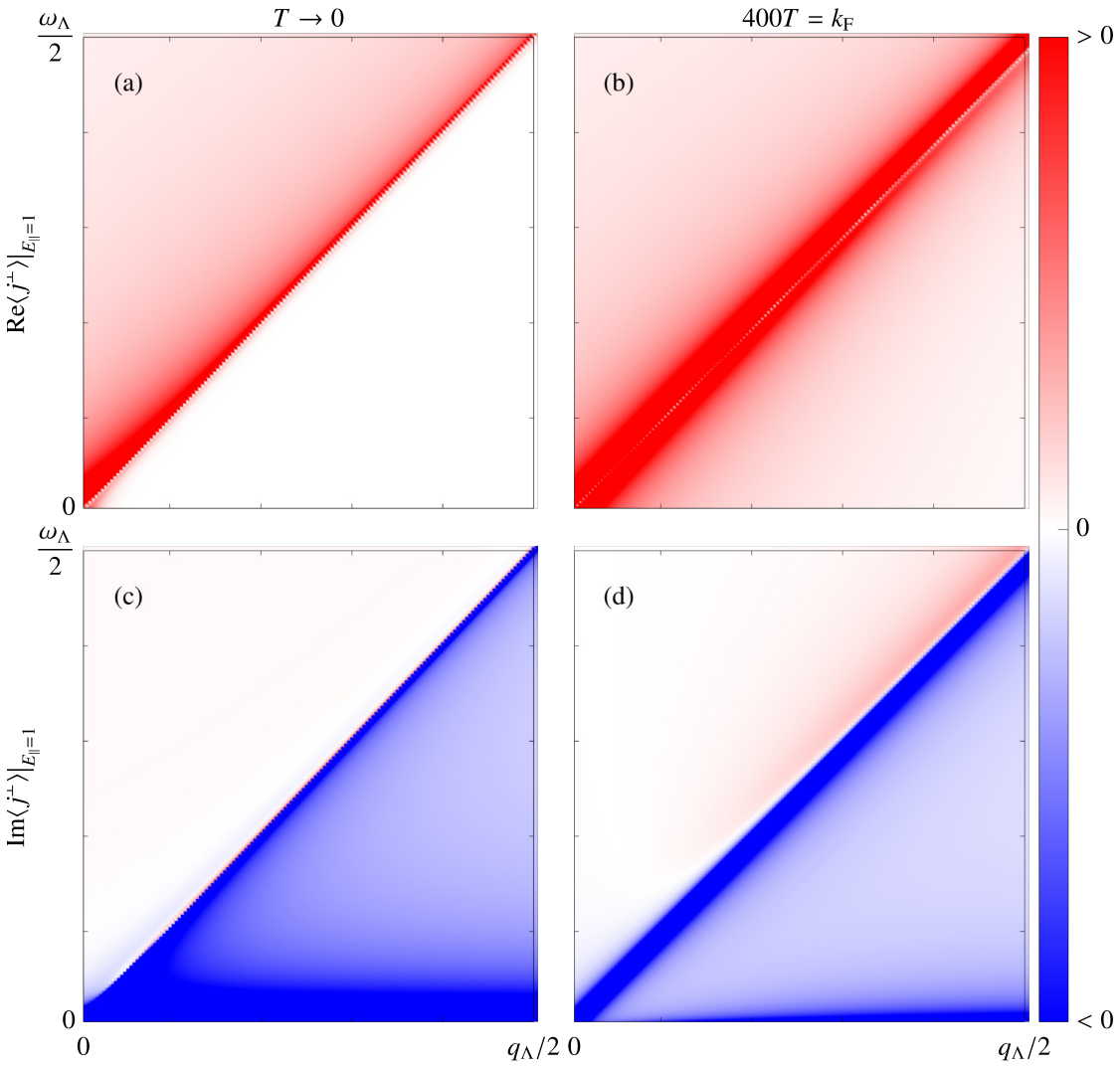

Figure 4.4: The current $\langle j^\perp \rangle$ evaluated for an external electric field tangential to the Fermi surface and fixed $q_\parallel = q_\Lambda k_F/10$. $q_\perp$ and ω range from 0 to $q_\Lambda k_F/2$ and $\omega_\Lambda k_F/2$ respectively to show the differences more clearly. (a) shows the real part of the subleading term in (3.30a) at $T \to 0$. (b) shows the same but at $400T = k_F$. (c) is the imaginary part of the current at $T \to 0$ and (d) is the imaginary part at $400T = k_F$. Red indicates positive values, and blue indicates negative values.

in (a) and (c) in figure 4.4 at $T \to 0$. We also find the expected pole running along the branch cut. As expected, there is also a $1/q_\perp$ pole at $\omega \to 0$. The imaginary part is negative, differing by a total sign when compared to (3.30a) which evaluates to a positive imaginary part. This is most likely due to some implicit branch choice made by Mathematica.

Unlike the leading term, there is now a visible change when turning up the temperature. The weight of the pole along $\omega = q_\perp$ increases with increasing temperature. The pole at $\omega = 0$ also diminishes with temperature. This behaviour can be seen

in figure 4.4 (b) and (d). While the pole above the branch cut remains for the real part, there is an additional pole that appears below a branch cut. The branch cut along $\omega = q_\perp$ seems to remain for the imaginary part, however. The conclusion is twofold; firstly, the subleading term in the currents $\langle j^t \rangle$ and $\langle j^\perp \rangle$ does have a temperature dependence as described. Secondly, the behaviour which appears in figure 4.4 (b) suggests an additional real term relevant in (3.30a), appearing only at $T \neq 0$ and $q_\parallel \neq 0$. Considering two-point functions, this behaviour indicates that the non-hydrodynamic subleading terms become dissipative at a finite temperature, even below the branch cut where, at zero temperature, there is no dissipation.

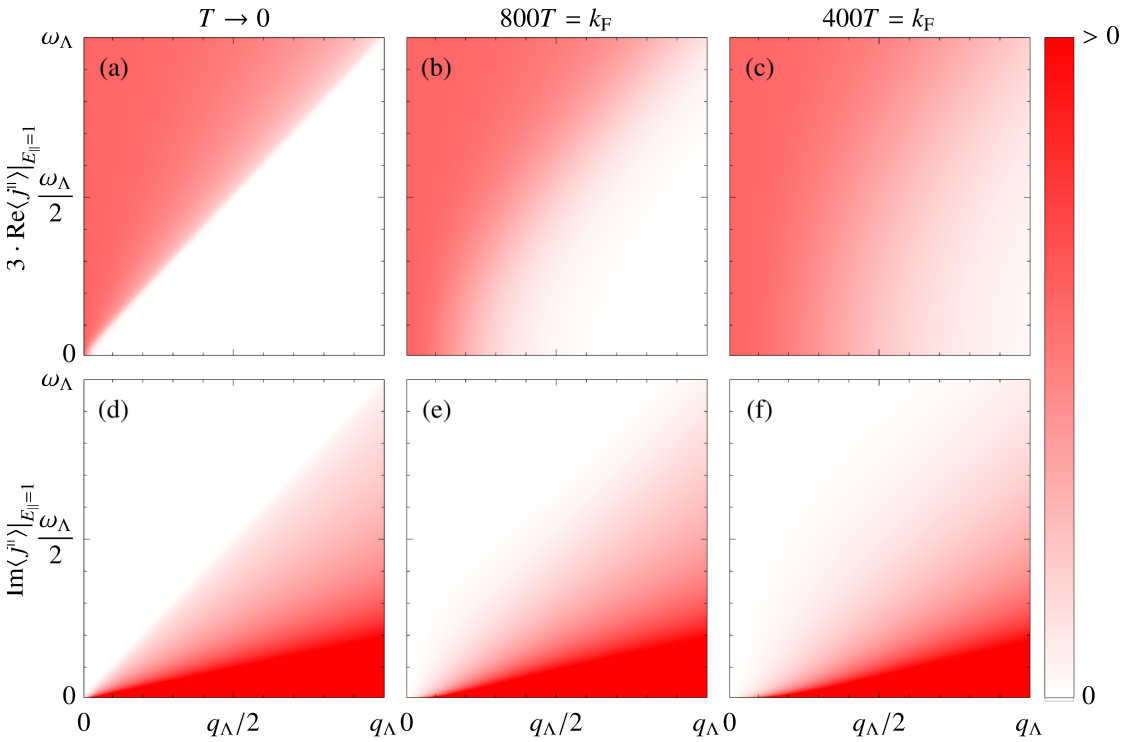

Figure 4.5: The current $\langle j^\parallel \rangle$ evaluated for an external electric field tangential to the Fermi surface at $q_\parallel = 0$. $q_\perp$ and ω range from 0 to $q_\Lambda k_F$ and $\omega_\Lambda k_F$ respectively. The top three figures,(a), (b), and (c), show the real part of $\langle j^\parallel \rangle$ at three different temperatures increasing from left to right. The bottom three figures, (d), (e), and (f), show the imaginary part at the same three temperatures increasing from left to right. Note that the real part has been multiplied to make the changes more apparent. The current at zero temperature has a constant continuum response of 1 that crosses a branch at $\omega = q_\perp$. Red indicates positive values, and blue indicates negative values.

Last is the k_F^0-term for $\langle j^\parallel \rangle$. The perturbing electric field is the same as for the subleading terms for $\langle j^t \rangle$ and $\langle j^\perp \rangle$, except that $q_\parallel$ can be set to zero. At zero temperature, the current has a strong response at $\omega \sim 0$, which increases for higher $q_\perp$. Beyond low ω, there is a continuum response equal to 1 ($3 \cdot 1$ in figure 4.5) until the expected branch cut at $\omega = q_\perp$ is reached, where the current goes from being imaginary to real. This can be seen in figure 4.5 (a) and (d). While similar, this is

not the exact behaviour we expect from (3.30b). We do not see any divergence at the branch cut as expected. This could be due to the higher-order terms contributing more to this term at the divergences. It could also be due to the fact that we are not actually at zero temperature but rather only approaching it. If the theory was pushed to $T = 0$, we may get back (3.30b). Furthermore, we see that there is the same sign difference in the imaginary part as was seen in figure 4.4. Again, we assume this to be due to an implicit branch choice by Mathematica.

As the temperature is increased, the biggest change is seen in the real continuum response. The sharp branch cut at $\omega = q_\perp$ vanishes and acquires a "width" as it slowly decreases from 1 to 0 for the real part. The decay is slower for higher temperatures. For the imaginary part, the cone shape at $\omega = 0$ is pushed forward in $q_\perp$ slightly, and the continuum increases slower with temperature with a "width" in a manner similar to the imaginary part. No matter the temperature or ω, the current is fixed at 1 at $q_\perp = 0$.

We can draw some conclusions about the behaviour at finite temperatures using the findings above. The properties associated with the hydrodynamics of any metal with a Fermi surface remain mostly unaffected at temperatures usual for metals. As for the properties unique to non-Fermi liquids, those being the k_{F}^0-terms in (3.30a) and (3.30b), the same can not be said. The temperature dependence manifests itself in a manner depicted in figure 4.4 and figure 4.5. As is argued in Ref. [21], this is an expected result. The leading term arises from the second term in (3.28), which decays exponentially with power $-k_{\mathrm{F}}r$. This is unlike the subleading terms which arise from the third term in (3.28), which decay with power $-r$. The behaviour of the leading term is thus determined near $z = 0$ when $k_{\mathrm{F}} \gg T$. In this region, the metric is very similar to the zero temperature metric. This is in contrast with the subleading terms, where the metric affects the physics more due to the slower decay of $-r$.

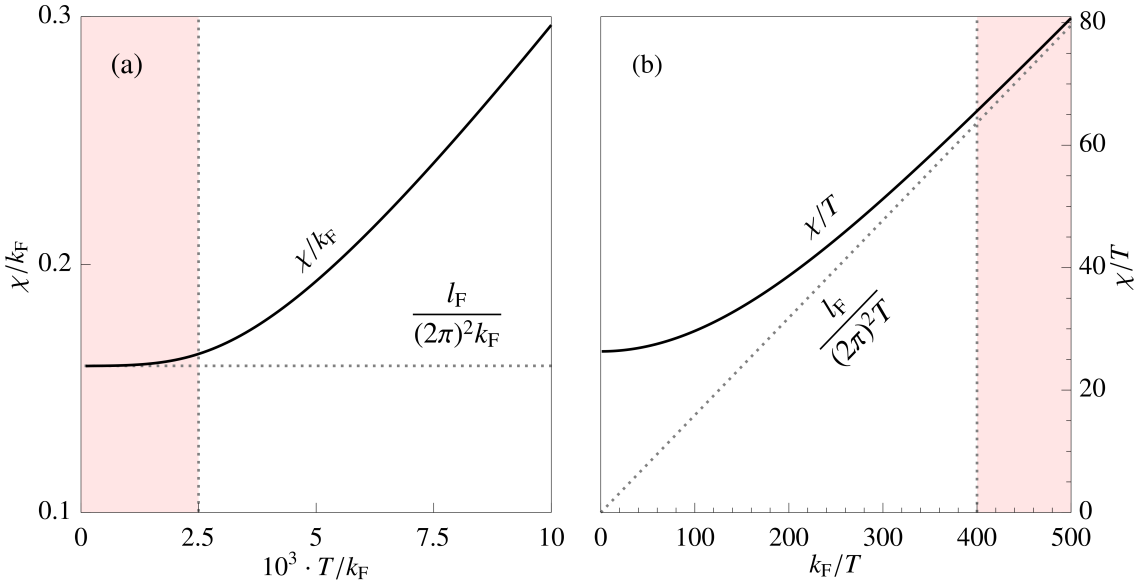

Figure 4.6: (a) shows the charge susceptibility as a function of temperature and (b) shows the charge susceptibility as a function of the Fermi energy. χ has been normalised in both figures by k_F and T respectively . The expected result is obtained for $k_F \to \infty$ or equivalently $T \to 0$. The red area is where $400T \leq k_F$.

4.2.1 Charge susceptibility

Unlike the currents above, we need to consider the contribution from the whole Fermi surface when evaluating the charge susceptibility. Doing so is not an issue since the equations of motion are ordinary in the radial coordinate. Thus, we can solve at each θ to get the local susceptibility at each point on the Fermi surface. First, we solve for the local susceptibility at each point on the Fermi surface separately at $N = 15$ points. This is akin to (3.32) where χ has a θ-dependence. Given χ at N points along the Fermi surface, we use a built-in function of Mathematica to interpolate between them. The result is the function $\int \mathrm{d}\theta' \chi(\theta, \theta')$. Finally, the interpolated function can be integrated over from 0 to 2π in θ, giving the charge susceptibility from the whole Fermi surface. Since we are evaluating at $\alpha = 1$ and $m = 1$ we expect from (3.33) to find

$$\chi = \frac{l_F}{(2\pi)^2} = [\text{For a circle}] = \frac{k_F}{2\pi} \tag{4.14}$$

at $T \to 0$. Indeed we see in figure 4.6 that for $T \ll k_F$ the susceptibility approaches $k_F/2\pi$. As the temperature increases, so does the charge susceptibility. Temperatures relevant for metals, meaning $400T \gtrsim k_F$, are within the zone marked in red. At $400T = k_F$ we find $\chi/k_F \approx 0.164$.

4.2.2 Optical conductivity

The optical conductivity is evaluated in the same manner as the charge susceptibility. Unlike the analytical case, however, we can evaluate the conductivity with the electric

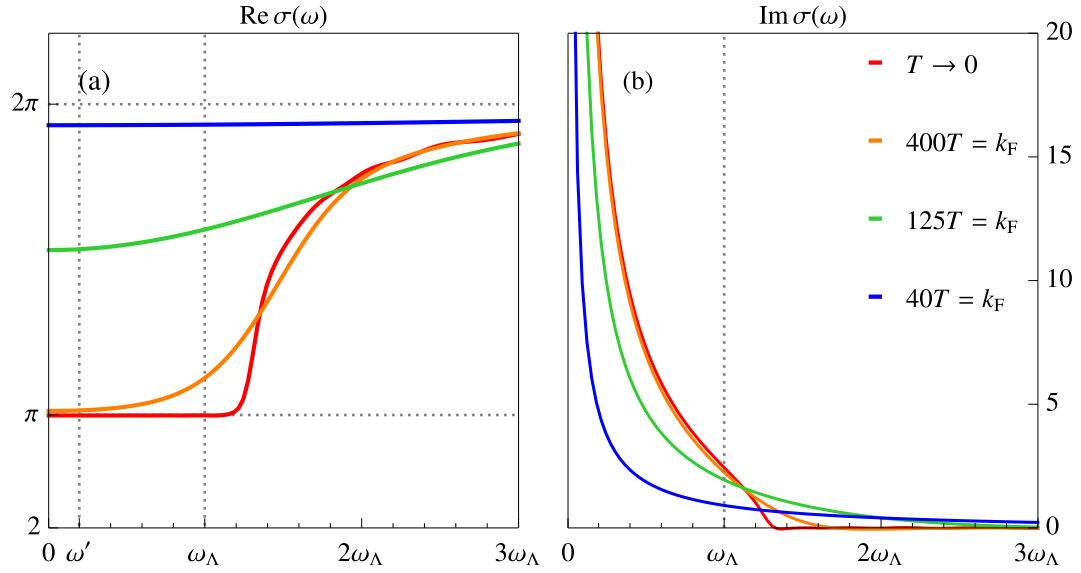

Figure 4.7: The numerical evaluation of the conductivity shown for four different temperatures. (a) shows the dissipative part of the conductivity, which includes the incoherent conductivity. At $T \to 0$ the conductivity is constant at π. As the temperature increases, the real part picks up a frequency dependence. No matter the frequency or temperature, (a) never exceeds 2π. (b) shows a Drude peak at $\omega = 0$ for all four temperatures. The Drude peak is mostly unaffected when beneath the cutoff and at temperatures $400T \leq k\mathrm{F}$.

field chosen to be in Cartesian coordinates. Turning on an electric field in the x direction we evaluate $\langle j^x \rangle$ at $N = 15$ points, on the Fermi surface. Interpolating at these N points gives a function in θ, which can be integrated over from 0 to 2π to give the conductivity contribution from the whole Fermi surface. At $T \to 0$ we see the expected imaginary infinite Drude peak at $\omega = 0$ associated with the translational invariance, as seen by the red line in figure 4.7 (b). There is little difference in the Drude peak for temperatures between $T \to 0$ and $400T = k_\mathrm{F}$ when $\omega/k_\mathrm{F} < \omega_\Lambda$. Next, we look at the real part as seen in figure 4.7 (a). When $\omega/k_\mathrm{F} < \omega_\Lambda$ at $T \to 0$, we see a constant incoherent conductivity, as shown by the red line. As the temperature is increased, a peculiar result is obtained; the real part picks up a frequency dependence. At temperatures or frequencies well beyond the cutoff, the real part of the conductivity asymptotically approaches 2π. As we saw in figure 4.5, the current tangential to the Fermi surface is constant at 1. Thus, some other terms contribute to the real part of conductivity at higher temperatures and frequencies.

Here, there are two interpretations: either the conductivity has a frequency dependence beyond the Drude peak that appears at higher frequencies and temperatures, or we have set a cutoff too high and are getting contributions from irrelevant terms. We see that the incoherent conductivity is approximately constant at energies where the frequency is comparable with the thermal energy, ω'.

5. Conclusion and outlook

We will conclude with a speculative discussion regarding two developments for the model. At $\omega = 0$, the theory has an infinite conductivity. While this is an expected result, it is unphysical, and we would like our system to have non-zero DC resistivity. Furthermore, the decoupling of the metric and gauge field means that the electromagnetic effects are unaffected by the stress-energy tensor. The metric must couple to the gauge field to capture thermoelectric effects. As a conclusion to this thesis, we will speculate what some plausible contenders might be to incorporate these effects into the theory.

5.1 Finite DC conductivity

As we saw in figure 4.7 (b), an infinite Drude peak was found at $\omega = 0$. The Kramers-Kronig relation tells us the real part will receive a contribution $K\delta(\omega)$, where K is some weight. We cannot see this peak in figure 4.7 (a), but it has to be there, hiding. As mentioned before, in holographic models for conductivity, translational invariance implies that there are no mechanisms in the bulk geometry that correspond to momentum relaxation of the boundary theory's charge carriers[8]. Carriers gain momentum from the electric field. If there is nothing to scatter the carriers they can continue accelerating under the influence of an electric field, leading to perfect conductivity.

In real materials, there is no continuous translational invariance. Even in the absence of impurities, the microscopic theory will have a lattice structure. A lattice gives a finite DC conductivity through a process called Umklapp scattering. Thus, the Drude delta function gets a width from the lattice structure, and the DC conductivity is no longer infinite. Indeed, introducing a background lattice through a spatially varying neutral scalar in the bulk to explicitly break continuous translational invariance is a common way to get finite DC resistivity in holography [65–67]. The scalar field backreacts on the metric and gauge field, forming a gravitational crystal.

In our case, the theory is precisely on the IR fixed point. Here, any resemblance of the lattice in the UV is an irrelevant perturbation that vanishes under RG flow. This means that when on the fixed point, the conductivity will be infinite, even if the theory has a microscopic lattice system. Recall that the G_{UV} could be comprised of lattice translations $\mathbb{Z}$ or continuous translations $\mathbb{R}$. The distinction makes no difference as both flow to the same IR theory. Thus, introducing a lattice in the bulk

[8] If the electric field does not depart any momentum on the system, this statement is not true. However, if such is the case, we are no longer describing compressible systems.

is not the correct approach.

A later development are the so-called axion models [67]. The axion linearly depends on spatial coordinates, thereby explicitly breaking translational invariance. Thus, these models introduce momentum dissipation without forming a lattice structure. While this approach seems more promising than the prior holographic lattice, we need to remember the source of the Drude peak. The Drude peak is caused by the continuous translation symmetry in the UV. For our effective theory, the UV regime does not exist. Instead, we describe the IR fixed point that originally flows from the UV. Having conserved momentum in the UV is partly what gives the emergent $G_{\mathrm{IR}} = \mathrm{LU}(1)$. Thus, the infinite Drude peak is caused by the conservation of the LU(1) symmetry and not by momentum conservation in the IR. If we want to suppress the infinite Drude peak, we will most likely need to partly break the LU(1) in a way corresponding to broken translational symmetry in the UV.

5.2 Coupling to metric fluctuations

As was seen in section 4.1, the metric fluctuations and gauge field fluctuations decouple completely in linear response theory. As the background of the gauge field is only dependent on θ, F will be linear in perturbations of the gauge field. The right-hand side of Einstein's equations, that being the stress-energy tensor $T_{\mu\nu} = F_{\mu\kappa}F^{\kappa}_{\nu} - \frac{1}{4}g_{\mu\nu}F_{\kappa\lambda}F^{\kappa\lambda}$, is quadratic in F, and therefore zero in linear response theory. Similarly, Maxwell's equations have a topological right-hand side from the Chern-Simons action where the metric perturbations cannot enter. The left-hand side is linear in F, and therefore linear in the perturbations. Thus, only the metric background affects Maxwell's equations, while Einstein's equations are completely unaffected by the gauge field. Electric and thermal transport generally couple together in charged quantum matter [17]. Thermoelectric conductivities are evaluated using two-point functions of both j^i and $\mathcal{T}^{ti}$, where $\mathcal{T}^{\mu\nu}$ is the stress-energy tensor dual to $g_{\mu\nu}$. As it stands, this theory will be unable to capture the interplay between electrical and thermal currents as $\langle j^{\mu}\mathcal{T}^{\nu\rho}\rangle = 0$.

The immediate way to counteract this would be to implement a background for the gauge field, which depends on any x_μ beyond its established θ dependence. Since we are considering an effective theory, this background should be relevant in the deep IR. One such possibility might be to introduce a B-field in the bulk. This would modify the background to become

$$A_i = k_i(\theta) - \frac{B}{2}\epsilon_{ij}x^i, \qquad A_t = A_r = 0. \tag{5.1}$$

The spatial indices i, j are raised and lowered by the identity, and $\epsilon_{xy} = 1$ is the antisymmetric symbol. When defining A_i as the Fermi surface, the identity was inferred from Fermi liquid theory by the relation $F_{\theta i} = \partial_\theta k_i(\theta)$. This relation still holds for (5.1) as the magnetic field term is an additive constant in θ.

There are two caveats to introducing a magnetic field that need to be considered.

Firstly, when making the identification for the Fermi surface from the anomaly equation, (3.12), we inferred the relation from Fermi liquid theory at $B = 0$. When $B \neq 0$, one might have to make a similar inference for the background for $F_{\theta t}$, which would modify A_t in our gauge. Secondly, we have assumed $j^\theta = 0$ at several points, as per LU(1) symmetry. In the presence of a magnetic field, however, we no longer have this identity. The non-conservation of LU(1) would have to be reflected in the left-hand side of the continuity equation by getting a contribution from $\partial_\theta j^\theta$. One way to do this may be to promote the A_θ to a dynamical field by considering a U(1) Maxwell theory on $M \times S^1$. Breaking LU(1) by introducing a magnetic field will likely also introduce a mechanism for momentum relaxation, giving finite DC conductivity. Even if this approach worked, it would only be a starting point. Ideally, we would want to formulate the theory in such a way that the metric fluctuations couple, even in the absence of a magnetic field.

While on the topic of speculation, one could consider the far more ambitious idea of abandoning the effective field theory and returning to the more common holographic approach of describing the entire RG flow from the UV to the IR. The aforementioned difficulties of DC conductivity and coupling to the metric really arise due to having to stay in the IR.

Concluding remark

Our findings show that the numerical solutions to the considered holographic model have behaviours that are mostly consistent with what is expected from the analytical calculations at zero temperature. The only deviation seen at $T \to 0$ is in the current tangential to the Fermi surface along the branch cut at $\omega = q_\perp$. This may be due to some behaviour lost in the approximations necessary for analytical calculations, or to the fact that T cannot actually be set to zero. As the temperature increases, the features general to ersatz Fermi liquids remain unchanged. However, for the properties unique to the non-Fermi liquid, which are the subleading terms arising from the strongly correlated physics indicated by branch cuts, a stronger temperature dependence appears. We claim that this model gives a promising foundation for a bottom-up model of a non-Fermi liquid. There are, however, some missing pieces. Key areas for future work include addressing the infinite DC conductivity and the coupling between metric and gauge fields.

References

[1] M. Cook. "Poincaré hyperbolic disk." (2006), [Online]. Available: `https://mathworld.wolfram.com/PoincareHyperbolicDisk.html`.

[2] M. D. Schwartz, *Quantum Field Theory and the Standard Model*. Dec. 15, 2013.

[3] M. E. Peskin and D. V. Schroeder, *An Introduction to quantum field theory*. Reading, USA: Addison-Wesley, 1995.

[4] F. J. Dyson, "The s matrix in quantum electrodynamics," *Physical Review*, vol. 75, no. 11, pp. 1736–1755, Jun. 1, 1949.

[5] M. A. Shifman, A. I. Vainshtein, and V. I. Zakharov, "QCD and resonance physics. theoretical foundations," *Nucl. Phys. B*, vol. 147, pp. 385–447, 1979.

[6] L. D. Landau, "The theory of a fermi liquid," *Zh. Eksp. Teor. Fiz.*, vol. 30, no. 6, p. 1058, 1956.

[7] P. Coleman, *Introduction to Many-Body Physics*. Cambridge: Cambridge University Press, 2015.

[8] H. v. Löhneysen, A. Rosch, M. Vojta, and P. Wölfle, "Fermi-liquid instabilities at magnetic quantum phase transitions," *Reviews of Modern Physics*, vol. 79, no. 3, pp. 1015–1075, Aug. 17, 2007.

[9] Y. Cao *et al.*, "Strange metal in magic-angle graphene with near planckian dissipation," *Physical Review Letters*, vol. 124, no. 7, p. 076 801, Feb. 18, 2020.

[10] N. D. Mathur *et al.*, "Magnetically mediated superconductivity in heavy fermion compounds," *Nature*, vol. 394, no. 6688, pp. 39–43, Jul. 1998.

[11] A. A. Patel, H. Guo, I. Esterlis, and S. Sachdev, "Universal theory of strange metals from spatially random interactions," *Science*, vol. 381, no. 6659, pp. 790–793, Aug. 18, 2023.

[12] S.-D. Chen *et al.*, "Incoherent strange metal sharply bounded by a critical doping in bi2212," *Science*, vol. 366, no. 6469, pp. 1099–1102, Nov. 29, 2019.

[13] J. M. Maldacena, "The large n limit of superconformal field theories and supergravity," *International Journal of Theoretical Physics*, vol. 38, no. 4, pp. 1113–1133, 1999.

[14] S. S. Gubser, I. R. Klebanov, and A. M. Polyakov, "Gauge theory correlators from non-critical string theory," *Physics Letters B*, vol. 428, no. 1, pp. 105–114, May 1998.

[15] E. Witten, *Anti de sitter space and holography*, Apr. 6, 1998.

[16] M. Ammon and J. Erdmenger, *Gauge/Gravity Duality: Foundations and Applications*. Cambridge: Cambridge University Press, 2015.

[17] S. A. Hartnoll, A. Lucas, and S. Sachdev, *Holographic quantum matter*, Mar. 20, 2018.

[18] J. Zaanen, Y. Liu, Y.-W. Sun, and K. Schalm, *Holographic Duality in Condensed Matter Physics*. Cambridge: Cambridge University Press, 2015.

[19] G. D. Mahan, *Many-Particle Physics*. Boston, MA: Springer US, 2000.

[20] S.-S. Lee, "Recent developments in non-fermi liquid theory," *Annual Review of Condensed Matter Physics*, vol. 9, no. 1, pp. 227–244, Mar. 10, 2018.

[21] D. V. Else, *Holographic models of non-fermi liquid metals revisited: An effective field theory approach*, Sep. 29, 2023.

[22] J. M. Luttinger, "Fermi surface and some simple equilibrium properties of a system of interacting fermions," *Physical Review*, vol. 119, no. 4, pp. 1153–1163, Aug. 15, 1960.

[23] D. V. Else, R. Thorngren, and T. Senthil, "Non-fermi liquids as ersatz fermi liquids: General constraints on compressible metals," *Physical Review X*, vol. 11, no. 2, p. 021 005, Apr. 6, 2021.

[24] N. Iqbal and H. Liu, "Luttinger's theorem, superfluid vortices and holography," *Classical and Quantum Gravity*, vol. 29, no. 19, p. 194 004, Aug. 2012.

[25] T. Faulkner and N. Iqbal, *Friedel oscillations and horizon charge in 1d holographic liquids*, Jul. 17, 2012.

[26] J. Polchinski and E. Silverstein, "Large-density field theory, viscosity and '2kf' singularities from string duals," *Classical and Quantum Gravity*, vol. 29, no. 19, p. 194 008, Aug. 2012.

[27] K. Skenderis, "Lecture notes on holographic renormalization," *Classical and Quantum Gravity*, vol. 19, no. 22, pp. 5849–5876, Nov. 21, 2002.

[28] I. Heemskerk and J. Polchinski, "Holographic and wilsonian renormalization groups," *Journal of High Energy Physics*, vol. 2011, no. 6, p. 31, Jun. 2011.

[29] T. Faulkner, H. Liu, and M. Rangamani, "Integrating out geometry: Holographic wilsonian RG and the membrane paradigm," *Journal of High Energy Physics*, vol. 2011, no. 8, p. 51, Aug. 2011.

[30] K. G. Wilson and J. Kogut, "The renormalization group and the expansion," *Physics Reports*, vol. 12, no. 2, pp. 75–199, Aug. 1, 1974.

[31] K. G. Wilson, "The renormalization group: Critical phenomena and the kondo problem," *Reviews of Modern Physics*, vol. 47, no. 4, pp. 773–840, Oct. 1, 1975.

[32] A. Altland and B. D. Simons, *Condensed Matter Field Theory*, 2nd ed. Cambridge: Cambridge University Press, 2010.

[33] J. Polonyi, "Lectures on the functional renormalization group method," *Open Physics*, vol. 1, no. 1, pp. 1–71, Jan. 1, 2003.

[34] M. Lassila, "Holographic duality and strongly interacting quantum matter," 2020.

[35] K. Schwarzschild, "On the gravitational field of a mass point according to einstein's theory," *Sitzungsber. Preuss. Akad. Wiss. Berlin (Math. Phys.)*, vol. 1916, pp. 189–196, 1916.

[36] J. M. Bardeen, B. Carter, and S. W. Hawking, "The four laws of black hole mechanics," *Communications in Mathematical Physics*, vol. 31, no. 2, pp. 161–170, Jun. 1, 1973.

[37] J. D. Bekenstein, "Black holes and entropy," *Physical Review D*, vol. 7, no. 8, pp. 2333–2346, Apr. 15, 1973.

[38] S. W. Hawking, "Particle creation by black holes," *Communications in Mathematical Physics*, vol. 43, no. 3, pp. 199–220, Jan. 1975.

[39] E. Lieb, T. Schultz, and D. Mattis, "Two soluble models of an antiferromagnetic chain," *Annals of Physics*, vol. 16, no. 3, pp. 407–466, Dec. 1961.

[40] M. Oshikawa, M. Yamanaka, and I. Affleck, "Magnetization plateaus in spin chains: "haldane gap" for half-integer spins," *Physical Review Letters*, vol. 78, no. 10, pp. 1984–1987, Mar. 10, 1997.

[41] M. Oshikawa, "Commensurability, excitation gap, and topology in quantum many-particle systems on a periodic lattice," *Physical Review Letters*, vol. 84, no. 7, pp. 1535–1538, Feb. 14, 2000.

[42] M. Oshikawa, "Topological approach to luttinger's theorem and the fermi surface of a kondo lattice," Oct. 4, 2000.

[43] F. D. M. Haldane, *Luttinger's theorem and bosonization of the fermi surface*, May 21, 2005.

[44] A. Pressley, G. Segal, A. Pressley, and G. Segal, *Loop Groups* (Oxford Mathematical Monographs). Oxford, New York: Oxford University Press, Jun. 9, 1988, 316 pp.

[45] Z.-C. Gu and X.-G. Wen, "Tensor-entanglement-filtering renormalization approach and symmetry-protected topological order," *Physical Review B*, vol. 80, no. 15, p. 155 131, Oct. 26, 2009.

[46] X.-G. Wen, "Colloquium: Zoo of quantum-topological phases of matter," *Reviews of Modern Physics*, vol. 89, no. 4, p. 041 004, Dec. 4, 2017.

[47] T. Senthil, "Symmetry-protected topological phases of quantum matter," *Annual Review of Condensed Matter Physics*, vol. 6, pp. 299–324, Volume 6, 2015 Mar. 10, 2015.

[48] D. V. Else and T. Senthil, "Critical drag as a mechanism for resistivity," *Physical Review B*, vol. 104, no. 20, p. 205 132, Nov. 29, 2021.

[49] R. Shankar, "Renormalization-group approach to interacting fermions," *Reviews of Modern Physics*, vol. 66, no. 1, pp. 129–192, Jan. 1, 1994.

[50] Wolfram Research, Inc. "Wolfram mathematica: Modern technical computing." (2024), [Online]. Available: `https://www.wolfram.com/mathematica/`.

[51] D. V. Else, "Collisionless dynamics of general non-fermi liquids from hydrodynamics of emergent conserved quantities," *Physical Review B*, vol. 108, no. 4, p. 045 107, Jul. 6, 2023.

[52] E. Nilsson, "Electron transport and collective modes in fermi and non-fermi liquids," Ph.D. dissertation, Chalmers University of Technology, 2024.

[53] J. M. Martin-Garcia *et al.* "xAct: Efficient tensor computer algebra for the wolfram language." (2002), [Online]. Available: `http://www.xact.es/`.

[54] J. M. Martin-Garcia, *xPerm: Fast index canonicalization for tensor computer algebra*, Mar. 6, 2008.

[55] D. Brizuela, J. M. Martin-Garcia, and G. A. M. Marugan, *xPert: Computer algebra for metric perturbation theory*, Jul. 6, 2008.

[56] J. M. Martin-Garcia. "xTensor: Fast abstract tensor computer algebra." (2020), [Online]. Available: `http://www.xact.es/xTensor/index.html`.

[57] J. M. Martin-Garcia. "xCoba: General component tensor computer algebra." (2020), [Online]. Available: `http://www.xact.es/xCoba/index.html`.

[58] J. P. Boyd, *Chebyshev and Fourier Spectral Methods: Second Revised Edition*. Courier Corporation, Dec. 3, 2001, 690 pp.

[59] A. Krikun, *Numerical solution of the boundary value problems for partial differential equations. crash course for holographer*, Jan. 4, 2018.

[60] A. Romero-Bermúdez, A. Krikun, K. Schalm, and J. Zaanen, "Anomalous attenuation of plasmons in strange metals and holography," *Physical Review B*, vol. 99, no. 23, p. 235 149, Jun. 25, 2019.

[61] T. Andrade, M. Baggioli, A. Krikun, and N. Poovuttikul, "Pinning of longitudinal phonons in holographic spontaneous helices," *Journal of High Energy Physics*, vol. 2018, no. 2, p. 85, Feb. 14, 2018.

[62] E. Nilsson, "Surface plasmon polaritons in strongly correlated media," 2021.

[63] M. Tornsö, "Plasma oscillations in holographic quantum matter," Ph.D. dissertation, Chalmers University of Technology, 2021.

[64] M. Rangamani, M. Rozali, and D. Smyth, "Spatial modulation and conductivities in effective holographic theories," *Journal of High Energy Physics*, vol. 2015, no. 7, p. 24, Jul. 2015.

[65] S. A. Hartnoll and D. M. Hofman, "Locally critical resistivities from umklapp scattering," *Phys. Rev. Lett.*, vol. 108, p. 241 601, 2012.

[66] G. T. Horowitz, J. E. Santos, and D. Tong, "Optical conductivity with holographic lattices," *Journal of High Energy Physics*, vol. 2012, no. 7, p. 168, Jul. 2012.

[67] A. Donos and J. P. Gauntlett, "The thermoelectric properties of inhomogeneous holographic lattices," *Journal of High Energy Physics*, vol. 2015, no. 1, p. 35, Jan. 9, 2015.

A. Example: Maxwell field

A calculation analogous to the scalar field in the bulk can be done for a U(1) gauge field. Now, however, a temperature is introduced for the boundary theory. We know from the dictionary that this corresponds to a black hole in the bulk. Assuming there is no backreaction on the metric from the gauge field, the action is given by the standard Maxwell action

$$S = -\frac{1}{4e^2}\int \mathrm{d}x^{d+2}\sqrt{-g}F^2 \tag{A.1}$$

where $F^2 = F_{\mu\nu}F^{\mu\nu}$ is the squared field strength tensor $F_{\mu\nu} = 2\partial_{[\mu}A_{\nu]}$. The metric background is now an AdS black hole solution,

$$ds^2 = \frac{L^2}{r^2}\left(-f(r)\mathrm{d}t^2 + \frac{\mathrm{d}r^2}{f(r)} + \mathrm{d}x^2 + \mathrm{d}\vec{y}^2\right). \tag{A.2}$$

Here, we have split the spatial coordinates. Whereas x previously denoted all spatial dimensions, it now only denotes one. The remaining $d-1$ spatial dimensions are denoted by $\vec{y}$. We drop the vector notation from here on, $\vec{y} \equiv y$. Varying (A.1) with respect to A_μ give the covariant Maxwell's equations

$$\partial_\mu\left[\sqrt{-g}g^{\mu\sigma}g^{\nu\rho}F_{\sigma\rho}\right] = 0. \tag{A.3}$$

There is a gauge freedom for A_μ; utilising this freedom, we choose the radial gauge, meaning $A_r = 0$. We make a plane wave ansatz, similar to the scalar field case, giving $A_\mu = a_\mu(r)\exp(-\mathrm{i}\omega t + \mathrm{i}kx)$, where we have chosen k to be along x without loss of generality. Using the ansatz in (A.3) gives the equations of motion for the different modes

$$\omega a_t' + kfa_x' = 0 \tag{A.4a}$$

$$a_t'' + \frac{2-d}{r}a_t' - \frac{k^2}{f}a_t - \frac{k\omega}{f}a_x = 0 \tag{A.4b}$$

$$a_x'' + \left(\frac{f'}{f} + \frac{2-d}{r}\right)a_x' + \frac{\omega^2}{f^2}a_x + \frac{k\omega}{f^2}a_t = 0 \tag{A.4c}$$

$$a_y'' + \left(\frac{f'}{f} + \frac{2-d}{r}\right)a_y' + \left(\frac{\omega^2}{f^2} - \frac{k^2}{f}\right)a_y = 0. \tag{A.4d}$$

We immediately notice that the equations of $a_\mu(r)$ decouple into the transverse modes $a_y(r)$ and coupled equations for the longitudinal modes $a_t(r)$ and $a_x(r)$. This calls for a simplification; by adding (A.4b) and (A.4c) with a prefactor of k and ω respectively,

$$\left(ka_t'' + \omega a_x''\right) + \omega\frac{f'}{f}a_x' + \frac{2-d}{r}\left(ka_t' + \omega a_x'\right) + \left(\frac{\omega^2}{f^2} - \frac{k^2}{f}\right)\left(ka_t + \omega a_x\right), \tag{A.5}$$

the equations for the longitudinal modes have almost been written in terms of a new variable $a_\parallel = ka_t + \omega a_x$. A hiccup in the first-order derivative term remains, which can be dealt with using (A.4a),

$$\begin{aligned}\omega\frac{f'}{f}a_x' &= \omega\frac{f'}{f}a_x' + \frac{k\omega f'\left(\omega a_t' + kfa_x'\right) + k^3ff'a_t' - k^3ff'a_t'}{\omega^2 f - k^2f^2} \\ &= \left(\frac{f'}{f} + \frac{ff'k^2}{f\left(\omega^2 - f^2f\right)}\right)a_\parallel'.\end{aligned} \tag{A.6}$$

The result is two decoupled differential equations for the Maxwell action

$$a_\parallel'' + \left(\frac{f'}{f} + \frac{ff'k^2}{f\left(\omega^2 - k^2f\right)} + \frac{2-d}{r}\right)a_\parallel' + \left(\frac{\omega^2}{f^2} - \frac{k^2}{f}\right)a_\parallel = 0 \tag{A.7a}$$

$$a_y'' + \left(\frac{f'}{f} + \frac{2-d}{r}\right)a_y' + \left(\frac{\omega^2}{f^2} - \frac{k^2}{f}\right)a_y = 0. \tag{A.7b}$$

All that is left to do is to go through the same song and dance as for the scalar field. Expanding $a_\parallel = a_\parallel^{(\Delta)}r^\Delta + \text{h.o.t}$ and $a_y = a_y^{(\Delta)}r^\Delta + \text{h.o.t}$ to find the asymptotic behaviour we solve for Δ in (A.7b) and (A.7b) in the limit $r \to 0$ giving

$$a_\mu(r) = a_\mu^{(0)} + a_\mu^{(1)}r^{d-1} \tag{A.8}$$

where μ in the radial direction still gives zero. The leading order is identified with the source. To compute the correlation functions using the GKPW rule, the on-shell action

$$S^\star[A_\mu] = -\frac{1}{2e}\int_{r=\epsilon}\mathrm{d}^{d+1}x\,\sqrt{-\gamma}n^\mu A_\mu^\star F^{\star\mu\nu} = \frac{1}{2e^2}\int_{r=\epsilon}\mathrm{d}^{d+1}x\,\frac{L^d}{r^2}\left(d-1\right)g^{\mu\nu}a_\nu^{(0)}a_\mu^{(1)} + \cdots, \tag{A.9}$$

is found identically to (A.9) with γ being the determinant of the induced metric and n^μ being the out-facing normal vector of the boundary. Unlike the scalar case, here, there are no divergences for the on-shell action as $\epsilon \to 0$. Finally, the GKPW rule can be used to evaluate the boundary currents

$$\langle j^t\rangle = \frac{\delta S^\star}{\delta a_t^{(0)}}\bigg|_{r=0} = -\frac{1}{e^2}L^{d-2}\left(d-1\right)a_t^{(1)} \tag{A.10a}$$

$$\langle j^i\rangle = \frac{\delta S^\star}{\delta a_i^{(0)}}\bigg|_{r=0} = \frac{1}{e^2}L^{d-2}\left(d-1\right)a_i^{(1)}. \tag{A.10b}$$

To explicitly evaluate the currents, we need to solve (A.7a) and (A.7b) for $a_\mu^{(1)}$, which has to be done numerically.

B. Numerics

The solutions to the equations of motion can be approximated using a series of Chebyshev polynomials T_n. In the pseudospectral method, we never explicitly do this. Instead, we immediately evaluate the perturbations on the Chebyshev-Lobatto grid from (4.8). Given the solution to a field $\phi(z_l)$ on the $\{z_l\}|_{l=1}^{l=N}$ grid points, we can solve for the coefficient of the first N Chebyshev polynomials from

$$\phi(z_l) = \sum_{n=1}^{N} a_n T_n(z_l), \qquad \sum_{n=1}^{N} a_n T_n(z) \equiv \phi_N(z) \xrightarrow[N\to\infty]{} \phi(z) \tag{B.1}$$

The reason for choosing Chebyshev polynomials T_n is because they converge to the correct solution of ϕ the fastest for a Dirichlet problem of our kind [58]. To ensure convergence to the solutions, we can inspect the convergence of the Chebyshev coefficients a_n. Ideally, we want $|a_N|$ to be several orders of magnitude smaller than $|a_0|$. If $|a_0|$ and $|a_N|$ are similar in size, then N is too small. if the difference is of order $\sim 10^8$ say, then the solution is probably accurate to many decimal places [58]. Checking the convergence of the Chebyshev coefficients is reliable for rejecting calculations whose accuracy is poor because N is too small. To trust our solutions, we should compare many N. If they give the same result, we can be confident in the results. We can see the convergence of the Chebyshev coefficients in figure B.1. The

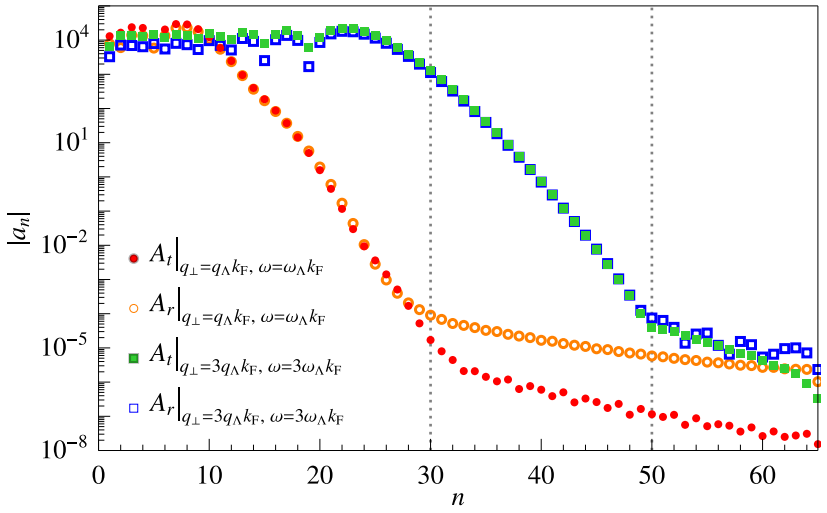

Figure B.1: Log-linear plot of the Chebyshev coefficients for A_t shown by the solid markers and A_r shown by the hollow markers. The circles show the coefficients to the solution of the gauge fields at $q_\perp = q_\Lambda k_F$ and $\omega = \omega_\Lambda k_F$, and the squares show the solutions for $q_\perp = 3q_\Lambda k_F$ and $\omega = 3\omega_\Lambda k_F$.

equations of motions are solved for at $T \to 0$. When at the cutoff q_Λ and ω_Λ, that we

chose, we see that the Chebyshev coefficients converge exponentially up until $n \sim 30$. The difference in orders of magnitude between $|a_0|$ and $|a_{30}|$ is about 10^9, meaning we can be confident in the accuracy of our solutions if it is the same for other N, which it is. When beyond the cutoff at $q_\perp = 3q_\Lambda k_\mathrm{F}$ and $\omega = 3\omega_\Lambda k_\mathrm{F}$, however, we see that the coefficients are yet to converge for $n = 30$. Instead, we see an exponential convergence that flattens out at $n \sim 50$. We can conclude that when working within our cutoff, we should have a Chebyshev-Lobatto grid with $N \gtrsim 30$; we set $N = 30$ to ensure accurate and fast convergence. When going past the cutoff, which we do when evaluating the conductivity, we must adjust N accordingly[9]; for $q_\perp < 3q_\Lambda k_\mathrm{F}$ and $\omega < 3\omega_\Lambda k_\mathrm{F}$ we set $N = 60$.

We could alternatively adjust the cutoff (4.12) and adjust N accordingly. Increasing N does, however, increase the run time of the evaluations. When $N = 30$, we have reasonable run times while keeping the cutoff above $400\omega = k_\mathrm{F}$ and $400q_\perp = k_\mathrm{F}$. We can, therefore, motivate the choice of cutoff as the q_Λ and ω_Λ such that $N = 30$ gives good convergence.

In figure B.2, the density two-point function from figure 4.1 is evaluated at $N = 30$ in (a) and $N = 60$ in (b) but now going beyond the cutoffs q_Λ and ω_Λ. We see how the numerics start to falter for $N = 30$ while $N = 60$ maintains the expected behaviour past the cutoff.

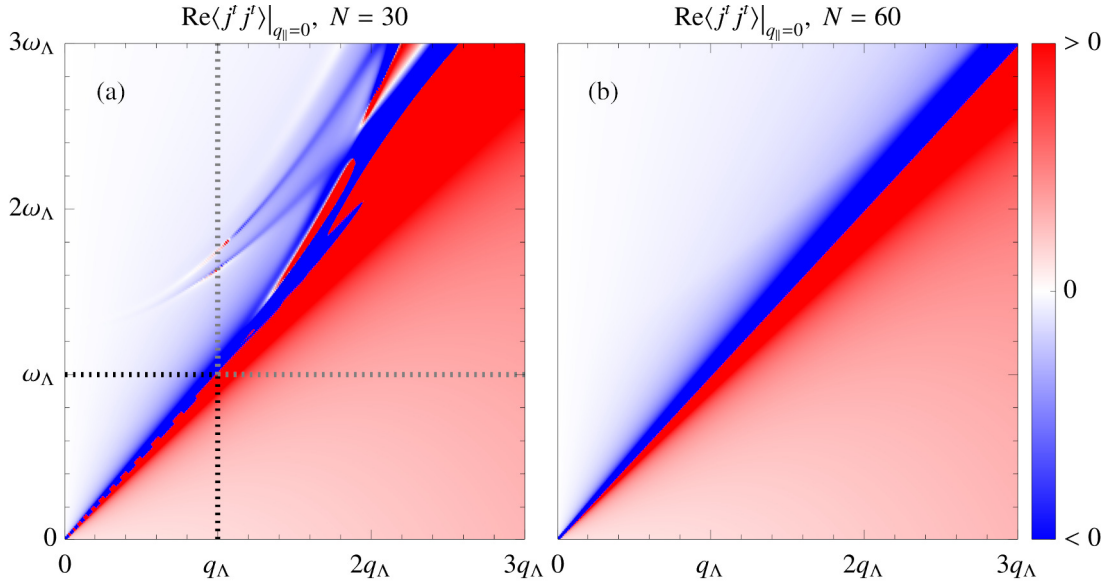

Figure B.2: The effect of the numerical calculations when choosing the density of the Chebyshev-Lobatto grid. In (a), we see $N = 30$; in (b), we see $N = 60$. The strange behaviour past the cutoff q_Λ and ω_Λ is corrected by increasing the number of grid points.

[9]Strictly speaking, this is not necessary for the conductivity since when $\mathbf{q} = 0$ the convergence is much better, allowing for smaller N.

DEPARTMENT OF PHYSICS
CHALMERS UNIVERSITY OF TECHNOLOGY
Gothenburg, Sweden
www.chalmers.se

CHALMERS
UNIVERSITY OF TECHNOLOGY